To the Graduate Council:

I am submitting herewith a dissertation written by Bernadeta Resti Widhiyatni Srijanto entitled "Implantable Piezoresistive Microcantilever-based Wireless Cocaine Biosensors". I have examined the final electronic copy of this dissertation for form and content and recommend that it be accepted in partial fulfillment of the requirements for the degree of Doctor of Philosophy, with a major in Electrical Engineering.

Paul B. Crilly, Major Professor

We have read this dissertation
and recommend its acceptance:

Thomas L. Ferrell

Michael J. Roberts

Marshall O. Pace

Accepted for the Council:

Dr. Carolyn R. Hodges
Vice Provost and Dean
of the Graduate School

(Original signatures are on file with official student records.)

Implantable Piezoresistive Microcantilever-based Wireless Cocaine Biosensors

A Dissertation

Presented for the

Doctor of Philosophy

Degree

The University of Tennessee, Knoxville

Bernadeta Resti Widhiyatni Srijanto

May 2008

Dedication

This dissertation is dedicated to my parents, my brother, and my sister back home.

Acknowledgments

I would like to thank Dr. Thomas L. Ferrell, who introduced me to biosensors and provided me with helpful ideas and criticism in this project; Dr. Paul B. Crilly for his encouragement and technical advice; Dr. Michael Roberts, and Dr. Marshall O. Pace for their assistance in this research and writing dissertation. Special thanks to for my co-workers Dr. Christine Cheney, David Hedden, and Anthony Gehl; my previous co-wokers Dr. Andrew Wig, the late Dr. Ed Arakawa; Dr. Hans Christen for useful discussions, and James Cantu who helped us in the "deprotecting" process of the aptamer.

I would also like to acknowledge the National Institute on Alcohol Abuse and Alcoholism (NIAAA) for the funding for this research under Contract No. N01AA23012 and the Department of Electrical Engineering and Computer Science, University of Tennessee Knoxville for providing me with financial support as graduate teaching assistant.

Abstract

Cocaine is a well-known, illegal, recreational drug that is addictive due to its effects on the mesolimbic reward pathway in the human body. Accurate and real-time measurement of the concentration of cocaine in the body as a function of time and physiological factors is a key requirement for the understanding of the use of this drug. Current methods for such measurements involve taking samples from the human body (such as blood, urine, and hair) and performing analytical chemistry tests on these samples. This techniques are relatively expensive, time consuming, and labor intensive. To address this issue, a new implantable sensor for the automated detection and measurement of the relative cocaine concentration is presented here. The device is more economical and provides for higher sampling frequencies than the current methods. The active sensor elements consist of piezoresistive microcantilever arrays, which are coated with an oligonucleotide-based aptamer, i.e. a short sequence of RNA with high affinity for specific target molecules, as the cocaine receptor. A Wheatstone bridge is used to convert the biosensor signal into an electronic signal. This signal is transmitted wireless at an operating frequency of 403.55 MHz, which complies with the US Medical Implant Communication System (MICS) FCC 47CFR Part 95. The limit of detection for the in vitro experiment is found to be 1 ng/ml. The device has successfully measured the relative concentration of cocaine upon implantation in the subcutaneous interstitial fluid of male Wistar rats.

Contents

List of Tables

List of Figures

Chapter 1

Introduction

1.1 Motivation

Measurement of the concentration of cocaine in the body as a function of time, dose and physiological factors is a core research focus in seeking to improve the understanding of the use of this drug. Correlation of cocaine use with the use of alcohol, nicotine, and other drugs is also a significant area of research. Hence, it is important to advance the state of the art in the science and technology of the measurement of cocaine concentrations in vivo. The present state of the art requires extracting blood or urine samples and performing analytical chemistry tests upon the withdrawn samples. Electrochemical tests are routinely used for the analytical assay. The process of drawing blood samples and analyzing them is clearly too expensive for high-frequency assessments over lengthy periods of time for large numbers of laboratory animals or human beings. In the case of laboratory animals, it is considerably easier to take samples at higher frequencies, but the cost is prohibitive regardless. In response to this condition, a low-cost implantable device that automatically reporting accurate and real time measurement of cocaine concentration is the key presented in this project.

Cocaine (benzoylmethyl ecgonine) is a well-known, illegal, recreational drug that is addictive due to its effects on the mesolimbic or reward pathway in the human brain. At

standard temperature and pressure (STP) cocaine is a crystalline tropane alkaloid that originates with the coca plant and certain South American native peoples are known to have chewed coca leaves as far back as hundreds of years ago. Cocaine in powder form is usually cocaine hydrochloride. Crack cocaine is cocaine with an increased amount of freebase cocaine. This can have a stronger and more rapid effect in the body. Orally administered cocaine requires almost 30 minutes to attain significant levels in the bloodstream and roughly 30 percent of the intake is typically absorbed. The peak effects of ingested cocaine occur after about one hour and the perceptible effects endure for about the same time span. Insufflation (sniffing) is the most often method of cocaine intake. Also, injection provides the most rapid onset of physiological effects on the central nervous system. Injection can actually be used in laboratory animals as small as fruit flies.

1.2 Goals and Expected Contributions

The challenges in developing a cocaine biosensor, which are mentioned in the previous section, involve the following characteristcs:

- inexpensive,
- simple,
- low-power,
- fast,
- sensitive, and
- small.

To achieve the above goals, this dissertation introduces a cocaine biosensor with active elements that consist of piezoresistive microcantilevers coated with an oligonucleotide-based aptamer as the selective cocaine binder. The micrometer size of the microcantilevers is the optimal selection for a small, implantable device that has all of the above characteristics.

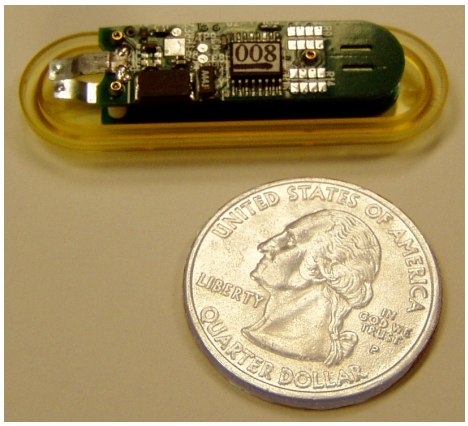

Figure 1.1: Our cocaine sensor placed next to a quarter.

The active elements are integrated with off-the-shelf electronic read-out components to produce a sensor with low cost, low power consumption, maximum battery life, and minimum complexity. The microcantilevers along with the electronic components are enclosed in an FDA-approved capsule as shown in Fig. 1.1. The sensor transmits its signal via telemetry to a receiver that is connected to a computer for data display. The success of this work has the potential to open a possibility for measurement of other drugs and biologically important compounds in the human body.

The accomplishments anticipated in this dissertation work are to have an optimized method for coating the microcantilevers with the cocaine receptor, to demonstrate in vitro cocaine detection for relative concentrations in different techniques, and to conduct in vivo sensor testing.

1.3 Previous Work on Cocaine Detection

1.3.1 Chromatography/Spectrometry

Cocaine in the human body has been measured by taking samples of urine [1], hair [2, 3] and sweat [4] from cocaine users. Saliva samples have also been used [5]. However, the saliva was taken from non-cocaine users and cocaine was then added for detection. Sun *et al.* reported a determination of cocaine in serum samples of rats after having been injected

with cocaine [6]. The analysis of the extracted cocaine from these samples was mostly done using gas or liquid chromatography incorporated with mass spectrometry, diode-arrays, and spectrophotometers. However, these techniques are quite complicated, time-consuming and expensive.

1.3.2 Electrochemical Analysis

Watanabe *et al.* explored a potentiometric electrochemical sensor by modifying the membrane between the electrodes in an electrochemical cell [7]. In improving the sensitivity and selectivity of the sensor, they incorporated a specific ion exchanger, sodium tetrakis [3,5-bis(trifluoromethyl)phenyl]borate (NaTFPB), and solvent mediator, tetrakis(2-ethylhexyl) pyromellitate (TEHPY), into a poly(vinyl chloride) (PVC) membrane between the electrodes. The pair of Ag,AgCl electrodes was connected to a high input impedance voltmeter to measure the electromotive force (emf) between the electrodes. The limit of cocaine measurement using this technique was found to be 0.4 μM (0.121 μg/ml).

Similar work was done by Campanella *et al.* using cocaine-reineckate or cocaine-tetraphenylborate as an ion exchanger [8,9]. The modified PVC membrane was attached to an ISFET (ion sensitive field effect transistor), which was fabricated by HEDCO Laboratory of Utah University. The modified ISFET device was immersed in cocaine solution, where ions of the cocaine solution were able to interact with the ion selective membrane. The challenge with this device was to keep the membrane adhered to the device. The ISFET measurements were carried out using a potentiometer Radiometer pH meter coupled to a recorder. The gate output voltage was recorded while keeping the source-drain current and drain potential constant using an opamp in a feedback loop. The limits of measurement were found to be 7 μM (2.12 μg/ml) for the cocaine-reineckate membrane and 15 μM (4.55 μg/ml) for the cocaine tetraphenylborate (TPB). Both were valid for pH range 2.5-7. For a 1 mM cocaine concentration, response times for the device were found to be less than or equal to 60 seconds.

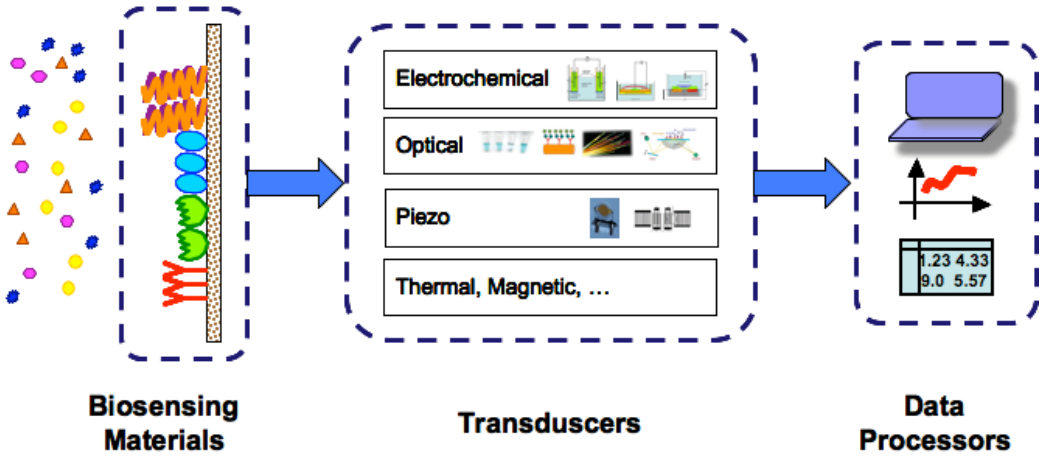

Figure 1.2: Block diagram of biosensor [10]. Note that Piezo includes piezoelectric and piezoresistive measurements.

1.3.3 Biosensors

Biosensors are sensing devices consisting of a biological sensing material and a chemical or physical transducer that converts a biological, chemical or biochemical signal into an electrical signal [10] (see Fig. 1.2). The biological sensing materials include enzymes, antibodies, nucleic acids (RNA and DNA), cells, receptors, tissues, etc. Transducers can be electrochemical, optical, piezoelectric, thermal, or magnetic types. In the present work the sensing material or coating is aptamer. Aptamers are DNA or RNA oligomers, specific lengths of the nucleic acid, that present a selective stereochemistry ("lock and key" structure).

Electrochemical biosensors

In contrast to the classical electrochemical sensor, an electrochemical-specific binding assay using antibodies as the biological sensing element has been investigated. Bauer *et al.* applied a non-competitive immunoassay using labeled alkaline phosphatase (ALP) anti-cocaine antibody as the cocaine binder [11]. First, cocaine in solution was mixed with the antibodies. After the excess antibodies were removed, the cocaine-antibody complexes were

passed into an amperometric detector. The electrode current was measured by a potentiostat and was recorded using a chart recorder. The limit of detection was 380 pM (0.115 ng/ml) of cocaine.

In work by Suleiman and Xu [12], benzoylecgonine-antibody and horseradish peroxidase (POD) enzyme were used as the cocaine binders. The binders were immobilized on a membrane mounted over the tip of an oxygen electrode. Current response of the electrode was recorded and cocaine measurement was found to be linear in the range of 0.1 μM to 10 μM (0.03 μg/ml to 3 μg/ml) with a working pH range of 5.8 to 8.2. This sensor can be regenerated by washing it with dilute hydrochloric acid solution and is stable for over 25 days.

A new class of molecules called aptamers has recently been introduced as the rival to the antibody [13]. As stated above, an aptamer is an oligonucleotide sequence with the capacity to recognize any class of target molecules with high affinity and specificity, and thus it can be used as a biological sensing element in biosensors.

An aptamer-based electrode sensor, called the E-AB sensor, was fabricated by Baker *et al.* [14]. The aptamer was immobilized on a gold electrode via the thiol group (-SH) creating a self-assembled monolayer. Current increased upon addition of the cocaine to the buffer solution where the electrode was immersed. Measurement limit was reported to be below 10 μM (3.03 μg/ml). The sensor was regenerated by immersing the electrode two times in a room temperature buffer for 3 minutes.

Optical-based biosensors

Optical-transducer sensors are based on absorption, surface plasmon resonance, luminescence, fluorescence, and optical fibers. Devine and co-workers developed a fiber-optic cocaine biosensor [15]. They used mAb antibody as the cocaine and cocaine metabolites binder. The antibodies were immobilized non-covalently on quartz fibers. The goal was to measure the evanescent wave fluorescence changes when cocaine or cocaine metabolites presented. A fluorescein conjugate of benzoylecgonine (FL-BE) was used to generate the

fluorescense. First, the FL-BE was flown onto the fibers and bound to the antibodies, and then the initial fluorescence was recorded. As cocaine or cocaine metabolites entered the fibers, it dissociated the bond of FL-BE and hence reducing fluorescence intensity in a concentration-dependent manner. Removal of cocaine allowed fiber regeneration. The limit of measurement was 5 ng/ml of cocaine and 30 ng/ml of benzoylecgonine metabolite.

Stojanovic *et al.* was the first to introduce an aptamer-based sensor for cocaine in solution [16]. The aptamer had a three-stem structure. This three-way junction was stable in the presence of cocaine. At the shortest end of these stems, they attached a 5' -fluorescein as the fluorophore and 3'-dabyl as a quencher. When exposed to cocaine solution, the aptamer behaved as a fluorescent sensor for cocaine. The purpose of the quencher was to reduce fluorescence intensity. Their experiment showed that without the quencher (fluorescein only) the fluorescence intensity remained constant with different concentrations of cocaine. They also showed that as the concentration of the cocaine was increased, the fluorescence quenching decreased. The measurement range was 10 μM to 400 μM (3.03 μg/ml to 121.36 μg/ml) cocaine concentration in serum.

In later work, Stojanovic and Landry replaced the use of the fluorophore and quencher with dyes [17]. They found that by adding a cyanine dye to the aptamer, they were able to observe significant changes in absorption maxima upon adding cocaine to the solution. The cocaine displaced the dye in the aptamer-dye complex, thus reducing the absorption peak detected by a spectrophotometer. The solution change of color was also visible by naked eyes. After 12 hours, a blue precipitate and partial decoloration of the solution was observed. The purpose of this method was to develop a sensitive and selective colorimetric sensor that was better than the corresponding fluorescent sensors. The limit of detection using this method was 0.5 μM (0.15 μg/ml).

A modification of Stojanovic's work was done by Liu and Lu [18]. They constructed gold nanoparticle aggregates functionalized with thiolated DNA. The particles were aggregated with linker DNAs. They observed a color change when cocaine was added to the solution due to disaggregation of the nanoparticles. The rate of color change increased with

increasing cocaine concentration. To confirm the color change observation, a UV/Vis spectrophotometer was used to detect changes in absorbance spectra. The advantage of this sensor from previous work was that the color change could be seen instantaneously upon adding the cocaine. Limit of detection was 50 μM (15.2 μg/ml) of cocaine.

Piezoelectric-based biosensors

Piezoelectric sensors use quartz crystal microbalance (QCM) and surface acoustic waves (SAW) as transducers. A piezoelectric device (PZ) is very sensitive in detecting a small mass change on its surface, which causes a measurable change in its resonant frequency, usually on the order of ng/Hz. Attili and Suleiman took advantage of this PZ property to detect cocaine [19]. Benzoylecgonine antibody, immobilized onto the gold electrode of a 10 MHz quartz crystal, was used as the cocaine binder. After its initial resonant frequency was recorded, the crystal was immersed in cocaine solution for 30 minutes then air dried and washed with distilled water. The shift in resonant frequency was then recorded to determine the binding mass of the cocaine. The measurement range was 10 to 300 μg/liter (0.01 to 0.3 μg/ml.

Similar work was performed by Halámek *et al.* [20, 21]. The gold electrode of a piezo crystal was first modified with BZE-DADOO, a derivative of cocaine. Different antibodies were tested to determine the best cocaine binder. Antibody was flown onto the crystal to obtain the initial or baseline resonance frequency of the crystal. For the cocaine detection, a mix of the antibody and cocaine was introduced onto the crystal. Change in resonance frequency was detected indicating the presence of cocaine. Regeneration the sensing surface of the crystal was conducted by flowing formic acid to the ligand-antibody complex. Limit of measurement was 34 ng/l (34 $\times 10^{-6}$ ng/ml) using the sheep antibody (IgG) and QCM with a smooth gold surface. Total time of one analysis was 15 minutes.

Frisk *et al.* developed a QCM sensor to detect cocaine in vapor phase [22]. The sensor contained a microfluidic vapor-to-liquid adsorption interface in a constant flow system with QCM detectors. Cocaine antibodies were immobilized on a gold electrode. Cocaine was

added to a dust collecting paper filter and was vaporized by heating the filter at 270^oC for 5 seconds. The cocaine vapor condensed on the liquid surface of PBS buffer which was flown into the system. When the cocaine passed the QCM, it bound to the antibody and released the antibody from the gold surface and thus increasing the resonant frequency of the QCM. The frequency shift recorded was 15 Hz for approximately 50 ng of cocaine sample.

Another cocaine sensor in vapor phase was introduced by Stubbs *et al.* [23, 24] using a surface acoustic wave (SAW) device. A SAW device is a piezoelectric-based device, and works in a similar principle as in QCM. However it has higher sensitivity than the QCM [10]. The primary part of this device was the two-port resonator, or the interdigital transducer (IDT). The ports consisted of aluminum electrode in a shape of interlocking combs and were fabricated on ST-X quartz with a center frequency of 250 MHz. The first port or the input IDT was used to convert the driving radio frequency signal into an acoustic wave, while the second port or the output IDT was used to convert the acoustic wave back to the RF signal to be fed back into an oscillator circuit. The sensor used anti-benzoylecgonine (anti-BZE) antibody as the cocaine binder. The antibody was immobilized on the electrodes on the device surface via protein-A cross linker. Cocaine vapor was generated using an INEL vapor generator. A shift of transient frequency was observed to determine the amount of cocaine bound to the electrodes. The device had a sensitivity of approximately 20 Hz/pg and its detection limit was on the order of a few picograms.

This work in measuring cocaine is summarized in the Table 1.1. The measurement unit is in $\mu g/ml$ unless otherwise stated.

1.4 Document Organization

This dissertation covers the development of the cocaine biosensor. Chapter 2 explains the background, theory, and mechanism of microcantilevers and surface stress-induced microcantilever deflection. Details of our cocaine sensor are described in Chapter 3. Several

Table 1.1: Summary of previous work on cocaine measurement.

Method	**Details**	**Meas. limit** ($\mu g/ml$)	**Ref.**
GC-LC/MS	serum (rat)	0.5×10^{-3}	[1]
	urine samples	0.1	[1]
	hair samples	$2–3\times10^{-3}$ μg/mg hair	[2, 3]
	sweat samples collected using patches	2.5×10^{-3} μg/patch	[4]
	saliva samples	5×10^{-3}	[5]
Electrochemical analysis	ion exchanger: NaTFPB solvent mediator: TEHPY membrane : PVC	0.121	[7]
	ion exchanger: cocaine-reineckate membrane : PVC	2.12	[8]
	ion exchanger: cocaine tetraphenylborate membrane : PVC	4.55	[9]
Electrochemical biosensor	receptor: alkaline phosphatase anticocaine antibody	0.12	[11]
	receptor: benzoyecgonine antibody and horseradish peroxidase enzyme	0.03	[12]
	receptor: cocaine aptamer [16]	3.03	[14]
Optical methods	Optical fibers	5×10^{-3}	[15, 25]
	Fluorescence	3.03	[16]
	Absorption: aptamer-dye complex	0.15	[17]
Piezoelectric-based	Quartz crystal microbalance (QCM) with antibodies	34×10^{-3}	[19–22]
	Surface acoustic wave (SAW) with antibodies	few picograms	[23, 24]

experimental setups are listed in Chapter 4. Chapter 5 we presents a discussion of the results. These are summarized in Chapter 6.

Chapter 2

Theory and Applications

In addition to their micrometer-size which advances the miniaturization of currently available sensors, microcantilevers have been demonstrated to have a very high sensitivity [26]. Furthermore, since microcantilevers are micromechanical devices, their fabrication uses standard methods for mass production of integrated circuits. The mass production combined with the advance of microfabrication technology leads to a low yield cost.

Before introducing more details about the cocaine biosensors, it is useful to understand the theory and background of microcantilevers, especially piezoresistive microcantilevers, and their mechanism as sensors which will be discussed in this chapter.

2.1 Microcantilevers

Microcantilevers were first used in atomic force microscopy (AFM) in 1986 to investigate the surface topography of an electrically insulating sample [27]. The cantilever was clamped at one end while a small tip was attached to the other end as sketched in Fig. 2.1. In this configuration, the tip almost touches the surface of a sample producing a force between the the tip and and the surface. This force causes the cantilever to bend. Since the AFM is allowed to moved in three dimensions, the cantilever bending is measured and is registered as topological information of the sample surface.

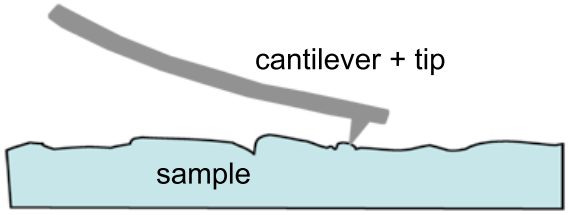

Figure 2.1: An AFM cantilever with a tip attached to it is used to image the surface of a sample.

Besides being used in scanning force microscopy, microcantilevers have also been used in a different field of interest, namely sensor applications. As sensors, mirocantilevers are very sensitive in detecting any changes of mechanical properties such as changes of cantilever mass, temperature, and surface stress. There are two methods to measure such changes [28, 29]: dynamic mode and static mode.

2.1.1 Dynamic mode

In the dynamic mode, the change in the resonance properties such as frequency, amplitude, and phase shift are measured. These property changes are usually caused by a change in mass of the cantilever as demonstrated in Fig. 2.2. Its resonance frequency, f (Hz), is given by [26]:

$$f = \frac{1}{2\pi}\sqrt{\frac{k}{m}} \tag{2.1}$$

where k and m are the spring constant (N/m) and the mass (kg) of the cantilever respectively. The value of the spring constant depends on the geometry and the material of the cantilever. For a rectangular cantilever displayed in Fig. 2.3, the spring constant is given by [26]:

$$k = \frac{EWT^3}{4L^3} \tag{2.2}$$

where E denotes the Young's modulus of elasticity for the composing material (N/m^2), and W, T, and L are the width, thickness, and length of the cantilever which are usually

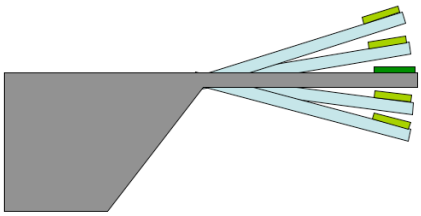

Figure 2.2: Illustration of resonant frequency changes due to change in mass applied on cantilever.

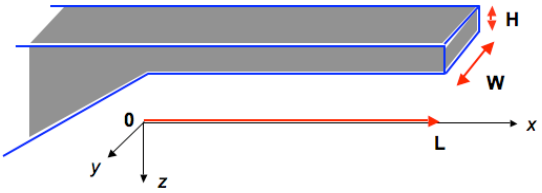

Figure 2.3: Beam cantilever or rectangular cantilever as used in the experiment.

in micrometers. To have a cantilever with a high sensitivity towards resonant frequency changes, a very stiff cantilever - hence, a high spring constant - is preferable.

The detection of resonance property changes due to a mass change has led to the development of gas sensors as described in Ref. [30–34]. In addition, the dynamic mode has been used in the tapping mode AFM where an oscillating cantilever's resonance properties change as it approaches a surface.

2.1.2 Static mode

The static mode measures the deflection or bending of cantilever. The amount of cantilever bending, z (m), for a given force, F (N), is defined in Hooke's law:

$$F = -kz \tag{2.3}$$

where k is the spring constant. To have a cantilever that gives maximum deflection for a given force, a soft cantilever with a low spring constant is preferable.

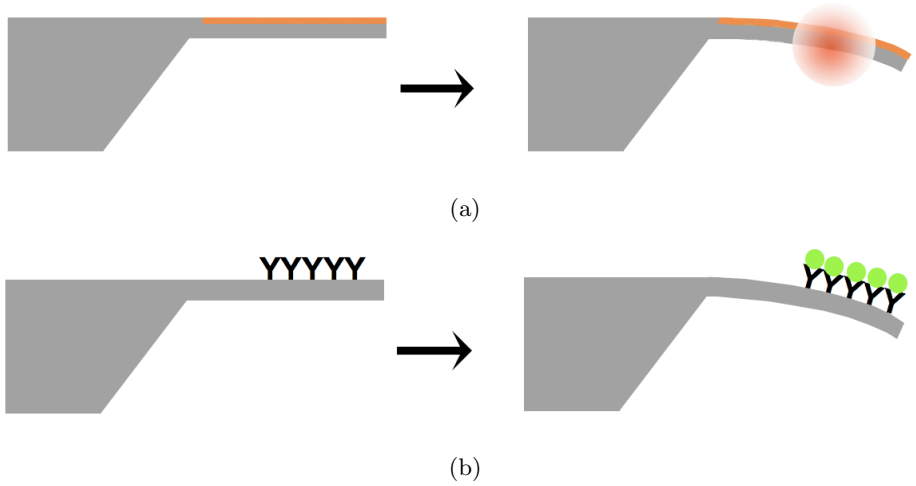

Figure 2.4: Origins of cantilever deflection in static mode. (a) Thermal effect. (b) Surface stress.

In AFM, the static mode is also called the contact mode. As introduced in Binnig's AFM [27], a force generated between the cantilever's tip and the surface of a sample as they touch each other causes the cantilever to bend.

The deflection can also be caused by a thermal effect or a surface stress applied to the cantilever as shown in Fig. 2.4. In the thermal-induced cantilever deflection, the cantilever is constructed using at least two different materials. The difference in the thermal expansion coefficient of the materials causes the cantilever to bend in one direction (the bimorph effect). Using this mechanism, Gimzewski *et al.* had designed a calorimeter to sense chemical reactions to be used in gaseous or vacuum environment [35]. The calorimeter was capable to detect heat changes as low as ∼1 picojoule and temperature changes as low as $\sim 10^{-5}$K at 300K. The device was then used by Barnes *at al.* to develop photothermal spectroscopy with femtojoule sensitivity [36].

The surface stress-induced cantilever deflection is caused by adsorption of molecules on a cantilever surface. This mechanism has been used to study the the mechanical properties of self-assembly monolayers of alkanethiols, particularly its formation process [37]. Fritz *et al.* demonstrated cantilever deflection in DNA hybridization. The cantilever was functionalized with a certain sequence of biomolecule or oligonucleotide followed by injection of the

complimentary oligonucleotide into the liquid cell resulting in hybridization. The cantilever was also capable of detecting a single base mismatch between two oligonucletides. Other molecular detectors based on the surface stress applied on microcantilevers are reported in Ref. [38–40].

2.2 Measuring microcantilever deflection

Tunneling method

There are several techniques to measure a microcantilever deflection. Binnig introduced the use of tunneling current in their AFM [27], as schematically displayed in Fig. 2.5(a). A diamond stylus tip is attached to one end of the cantilever and they are integrated with a scanning tunneling microscopy (STM)*

Their AFM operates using a similar principle as the STM. However, instead of keeping the tunneling current constant between the tip and the sample, it maintains a constant force between them. This operation mode makes scanning of non-conducting samples possible. The cantilever and the diamond stylus are placed between the surface of a sample and the STM tip. The AFM sample is mounted to a three-dimensional piezoelectric drive in x, y, and z direction. The sample is modulated in the z direction. As the stylus is brought to a very close distance to the sample, the force between the sample and the stylus causes deflection the cantilever which results in the tunneling current to vary. The modulated tunneling current is used to control the AFM feedback circuit in maintaining the constant force.

*STM is another method to scan surface topography of conducting samples, invented before the AFM also by Binnig *et al.* [41]. When a very sharp tungsten tip is brought close to the Pt surface with approximate distance of 1 nm tunneling current flows from the tip to the surface. The movement of the tip is controlled by piezodrives, P_z and P_y. The goal is to keep the tunneling current constant. To obtain this goal, a control unit is attached between the tip and piezodrive P_z. When the tip moves due to surface change, the control unit adjusts the voltage of the piezodrive P_z to keep the tunneling current constant. The voltages of the piezodrives P_z, P_y, and P_z are registered as the topography of the sample surface.

Capacitance method

Göddenhenrich *et al.* introduced a capacitance method to measure cantilever deflection used in their magnetic force microscope (MFM) design [42]. An aluminum microtip is attached to a V-shaped lever which is fabricated from 25 μm aluminum wires and has a calculated spring constant of 1 N/m. One of the capacitor plates is placed on the microtip, while the opposite capacitor plate is mounted on a controlled piezo tube. Both plates are made of aluminum foil and have dimensions of $300\mu m \times 300\mu m$. The sample is mounted on a single-tube x, y, z scanner which allows lateral scan width of 10 μm and a vertical deflection of 1 μm. During scanning, the force-induced lever deflection causes the capacitance to change due to change of the distance between the capacitor plates. A transformer bridge with a ratio 100:1 and a phase-sensitive lock-in amplifier are used for the capacitance detection. The device sensitivity is found to be 10^{-6} pF for 0.001 nm distance change between the plates. Fig. 2.5(b) shows the schematic diagram of this method whose applications are capacitance imaging and investigation of magnetic properties of materials.

2.3 Optical methods for measuring microcantilever deflection or resonance properties

Optical techniques can be used in the dynamic or static mode detection. Martin *et al.* [43] presented a modified version of atomic force microscopy which measures the force between a tip and a sample as a function of the distance between the tip and the sample surface. A tungsten tip is tethered at the end of a wire which serves as the cantilever. This cantilever is mounted on a piezoelectric transducer. The transducer vibrates the tip at the cantilever's resonant frequency. The tip, cantilever, and the transducer are integrated with a He-Ne laser heterodyne interferometer used to measure the vibration amplitude [44]. The laser beam from the interferometer applied onto the surface of the cantilever is reflected and interfered with a reference beam producing a photocurrent on a photodetector with a frequency determined from the frequency difference between both beams. As the tip is

brought at a close proximity to the sample surface, the amplitude of the vibration changes due to the shift of cantilever resonant freqency, resulting in a phase modulation of the photodetector current. The applications of this method are material sensing and surface profiling.

Another interferometric-based detection method, called the differential interferometry, used to measure a force-induced cantilever bending in force microscopy is presented by Schönenberger and Alvarado [45]. A cantilever is fabricated by cutting it out of GaAs wafer that has been ground and chemically etched. The tip is made of a piece of tungsten wire and is glued to one end of the cantilever using a conductive epoxy. The back of the cantilever is polished and coated with gold to facilitate reflection of two laser beams referred as the reference beam and the sensing beam. The sensing beam is reflected off the cantilever end near the tip, while the reference beam is reflected at the side of the shaft where the cantilever is mounted. The reflected beams are detected by two photodiodes which convert the intensity of the beams into electrical signals.

Sarid *et al.* reported a compact detection scheme using a single-mode GaAlAs double-heterostructure semiconductor laser diode emitting at 780 nm [46]. The beam reflected off the cantilever surface is detected by a photodiode where the ac current is proportional to the vibration amplitude of the cantilever. Meyer and Amer [47] proposed another simple optical-based scheme for detecting cantilever bending used in atomic force microscope. The cantilever is made of 75 μm tungsten wire and is electrochemically etched to form a sharp tip at the end. A minute mirror ($300\mu m \times 300\mu m$) is placed on the backside of the cantilever to reflect the laser beam which off the cantilever. The reflected beam is captured by position-sensitive detector (PSD) whose output is measured using a phase-sensitive device. A general mechanism of the optical methods for measuring microcantilever deflection or resonance properties is schematically displayed in Fig. 2.5(c).

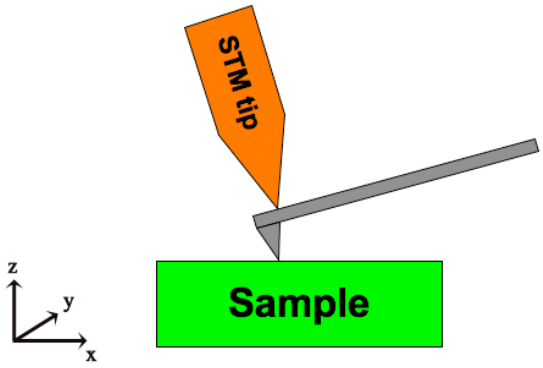

(a)

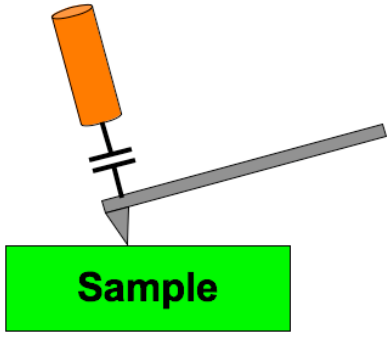

(b)

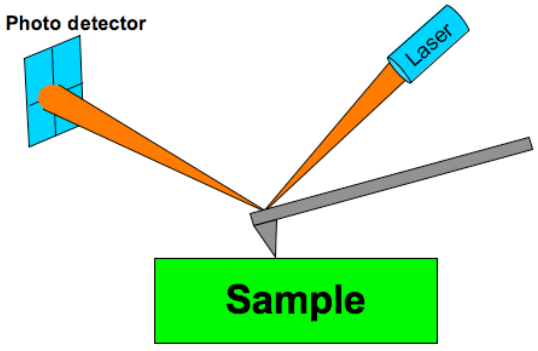

(c)

Figure 2.5: Methods of measuring cantilever deflection. (a) Tunneling current method. (b) Capacitance method. (c) Optical-based method.

Table 2.1: Different methohds of measurement changes in cantilever properties.

Mode	Source	Method
Dynamic	Shift in resonance properties due to mass (shift in amplitude, frequency, and phase)	Optical
Static	Deflection due to thermal or surface stress	Tunneling Capacitance Optical Piezoresistive

2.4 Piezoresistive microcantilevers

Although the techniques described above offer advantages such as high sensitivity and noise immunity, they are impractical for sensor applications because the complete instruments are usually large in size and complicated due to their external sensor components. In addition to being expensive, adjustment or alignment of the cantilever and the optical detector is usually time consuming.

In 1991, Tortonese *et al.* proposed a new detection scheme to measure cantilever deflection. The deflection sensor, which used a varying resistance (i.e. piezoresistive material), is embedded in a microcantilever [48] as demonstrated in Fig. 2.6. The piezoresistive cantilevers are made of a p-doped channel in silicon nitride, which exhibits a strong piezoresistive effect. The cantilever is connected to an external DC-biased Wheatstone bridge as sketched in Fig. 2.7. The bridge directly measures the voltage across it which is proportional to the value of the resistance change due to the cantilever bending.

The different methods in measuring the changes in cantilever properties as listed above are summarized in Table 2.1.

In Section 2.5, different mechanisms are discussed which result in the bending of a cantilever not due to its interaction with a surface of the sample, but because of elastic stress resulting from the binding of molecules at the surface.

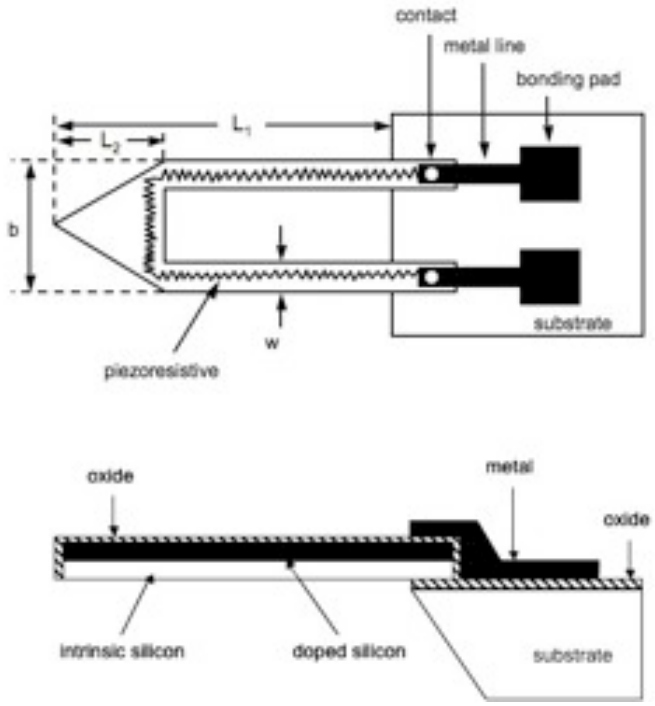

Figure 2.6: Triangular shape piezoresistive microcantilever introduced by Tortonese *et al.* from Ref. [48]

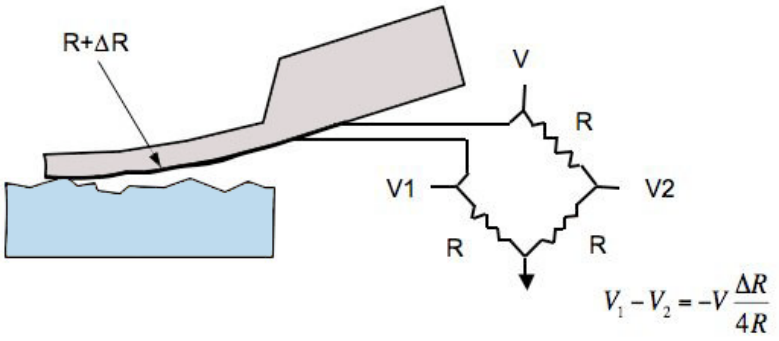

Figure 2.7: The piezoresistive microcantilever is connected with a Wheatstone bridge to measure the change in the resistance of the piezoresistive material when the cantilever deflects from Ref. [48]

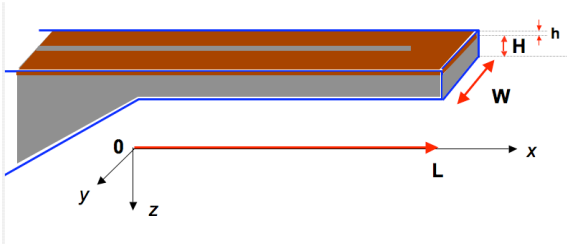

Figure 2.8: Beam cantilever or rectangular cantilever with a thin film (i.e. piezoresistor) deposited on it.

For any given rectangular cantilever as shown in Fig. 2.8, the amount of cantilever bending due to surface stress is defined using Stoney's formula [49]:

$$z = \sigma_s \frac{3L^2(1-\upsilon)}{EH^2} t \tag{2.4}$$

where z is the amount of cantilever bending (m), σ_s is the surface stress $(\mathrm{N/m^2})$, E is Young's modulus $(\mathrm{N/m^2})$, υ is Poisson's ratio, L and H are the cantilever length and thickness respectively, and t is the thickness of thin film deposited on the cantilever (i.e. piezoresistive material). However, $t \ll H$.

A mathematical derivation of Eq. 2.4 can be found in Ref. [29], in which a spring constant for surface stress-induced microcantilever, k_{σ_s}, was deduced by inserting z in Eq. 2.4 into:

$$\sigma_s = k_{\sigma_s} z \tag{2.5}$$

resulting in

$$k_{\sigma_s} = \frac{EH^2}{(1-\upsilon)3L^2} \tag{2.6}$$

A typical spring constant for a stress-induced microcantilever deflection is in the range between 1 mN/m to 1 N/m [50]. A 1 mN/m surface stress experienced by a microcantilever contributes to a bending of 1.6 nm.

For a piezoresistive material on which a strain is applied, the value of its resistivity changes. For a rectangular piezoresistor with a pathway for a current flow demonstrated in

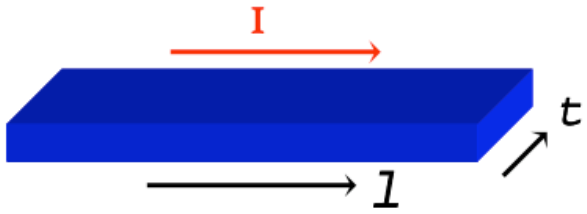

Figure 2.9: Rectangular-shaped piezoresistor adapted from Ref. [29]. The longitudinal direction is along the current flow, while the transversal direction is perpendicular to the current flow.

Fig. 2.9, its sensitivity, which is the relative change in resistance, is defined by [29]:

$$\frac{\Delta R}{R} = K_l \varepsilon_l + K_t \varepsilon_t \tag{2.7}$$

where K is the gauge factor, which is a material parameter, ε is strain applied to the cantilever, and the subscripts l and t represent longitudinal and transversal direction of the cantilever with respect to the direction of the current flow. Both the gauge factor and strain are dimensionless quantity. They have no units of measure.

Fig. 2.10 illustrates the geometry and placement of the piezoresistor relative to the cantilever that is used in the experiment. The current flows from one leg of the piezoresistor to the other, through the top part. The piezoresistive then can be divided into two components, i.e. the legs and the top part:

$$\frac{\Delta R}{R}_{total} = \frac{\Delta R}{R}_{legs} + \frac{\Delta R}{R}_{top} \tag{2.8}$$

$$= (K_l \varepsilon_x + K_t \varepsilon_y) + (K_l \varepsilon_y + K_t \varepsilon_x) \tag{2.9}$$

where $\frac{\Delta R}{R}_{legs}$ represents both legs of the piezoresistor. In a simplified case, where the top part resistance is negligible compared to the total resistance, the total relative change in

Figure 2.10: Geometry of the piezoresistor on the cantilever adapted from Ref. [29] with direction of the current shown.

resistance can be shown to be:

$$\frac{\Delta R}{R}_{total} = K_l \varepsilon_x + K_t \varepsilon_y \tag{2.10}$$

The strain for an elastic isotropic material is given by [51]:

$$\varepsilon_x = \frac{1}{E}(\sigma_x - \nu(\sigma_y + \sigma_z)) \tag{2.11}$$

$$\varepsilon_y = \frac{1}{E}(\sigma_y - \nu(\sigma_x + \sigma_z)) \tag{2.12}$$

where σ denotes the stress, E and ν are the Young's modulus and Poisson's ratio of the material respectively. For a uniform in-plane stress applied on a cantilever, the stress out of the plane of the cantilever, σ_z, is zero and $\sigma_x = \sigma_y$ which leads to:

$$\varepsilon_x = \varepsilon_y = \frac{\sigma_x}{E}(1 - \nu) \tag{2.13}$$

Inserting ε_x from Eq. 2.13 into Eq. 2.10, the sensitivity of the cantilever can be written as:

$$\frac{\Delta R}{R} = [K_l + K_t](1 - \upsilon)\frac{\sigma_x}{E} \tag{2.14}$$

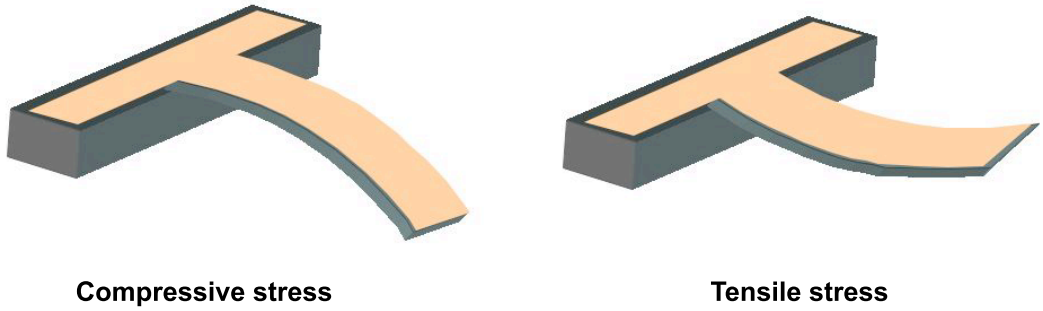

Figure 2.11: The bending direction of a microcantilever as a result of stress in the coating layer. Deflecting away from the top surface is related to compressive stress; deflecting toward the top surface is related to tensile stress.

Eq. 2.14 clearly shows the relation of surface stress with change in resistivity, as needed for this work.

2.5 Surface Stress - Transduction mechanism

If one side of the cantilever is coated with a different material, the involved stress will result in cantilever deflection. The direction of the deflection depends on the stress in the coating layer as illustrated in Fig. 2.11:

1. Compressive stress, where a cantilever bends away from its top surface.

2. Tensile stress, where a cantilever bends toward its top surface

Details on how molecular recognition or attachment to a cantilever can cause surface stress and which direction the cantilever deflects due to the molecular binding are still being studied and investigated. There are several theories regarding this phenomenon.

2.5.1 Electrostatic repulsive force

Berger *et al.* [37] immobilized alkanethiols on a V-shaped silicon nitride cantilever that had been coated with 20-nm gold, creating a self-assembled monolayer. The process was monitored and the cantilever bend was observed using a scanning force microscope technique. The results showed a range of cantilever deflection between 50 to 200 nm away from its top surface. This number is much greater than the deflection caused by the thermal effect, which is only ∼0.5 nm [35], and that caused by changes in mass due to molecular loading, which is ∼5 pm. Based on these negligible numbers, they concluded that the chemisorbed alkanethiols produce a compressive surface stress during self-assembly. They also reported that the stress is proportional to the number of molecules adsorbed on the gold and to the length of the alkyl chain. They explained that the compressive stress is due to electronic repulsion of the alkanethiol. When the thiol attaches to the gold surface, it creates an apparent dipole moment: $Au^+ - S^-$ and $S^- - alkyl^+$. Therefore, as the alkyl chain gets longer, the apparent dipole moment also gets larger, results in increasing electrostatic repulsion. The typical amount of surface stress due to the dipolar repulsive force of adsorbate and adsorbant is 10^{-3} N/m [52].

A similar experiment was done by Fritz *et al.* [53] by immobilizing a thiol-modified oligonulectides on a gold-coated cantilever for DNA hybridization and detection of a single base mismatch of two DNA sequences. They observed a compressive surface stress of 5 mN/m during DNA hybridization, which is ∼100 times smaller than the stress resulting from the alkanethiol immobilization done by Berger *et al.* above. Fritz *et al.* also suggested that the electrostatic repulsive force is responsible for the surface stress. This force is due to negative charges from the sugar-phophate backbone of the oligonucleotides.

2.5.2 Entropy

Wu *et al.* [54] reported that in addition to the electrostatic repulsive force between neighboring DNA chains, the cause of cantilever bending is also due to a change in configurational

entropy. Two experiments were conducted, an immobilization of single-stranded DNA (ssDNA) on a gold-coated microcantilever followed by a DNA hybridization. During ssDNA immobilization the microcantilever bent away from its top surface or downwards. Hence, the microcantilever experienced a compressive stress which can be explained using the electrostratic repulsive force theory as suggested by Fritz *et al.* During DNA hybridization, on the contrary, the microcantilever bent toward its top surface or upwards instead of having larger deflection away from the surface as one would have expected. This phenomenon can not be explained using the repulsive force theory alone. In general, single-stranded DNA chains will gain maximum configurational entropy in a free solution. However, when they are attached onto a cantilever surface and are placed in a very close distance with their neighboring chains, the conformational entropy decreases. As the counterbalance, the decrease in the entropy leads to an increase in the driving entropy force resulting in forming cantilever curvature. When the complementary target ssDNA are introduced, the hybridization process created rod-like double-stranded DNA chains with reduced configurational entropy driving force. Consequently, a smaller curvature is formed producing an upwards cantilever deflection.

Despite the considerable interest and amount of work focused on an understanding of how the binding of molecular species at the cantilever surface result in its bending, open questions remain. Alternative explanation may need to be considered. For example, Liu *at al.* suggest that flexoelectric bending of the cantilever material, induced by the bound charges at its surface, is the dominant mechanism [55]. In fact, these authors show that published results of cantilever bending in [54, 56, 57] can be explained by this mechanism.

Chapter 3

Design of the Cocaine Biosensor

The complete cocaine sensor system described in this work is divided into two parts: a sensor device, which will be referred to as sensor in the rest of this dissertation, and a receiver set, called the base station. The sensor is a monitoring device that detects cocaine in the human body. It communicates wirelessly with a receiver, the base station, linked to a computer (PC) serving as a user interface via USB connection. Fig. 3.1 and Fig. 3.2 illustrate a conceptual drawing and the block diagram of the cocaine sensor system. More than one sensor is allowed to communicate with one base station. Each sensor may be placed up to 10 meters from the base station. The operating frequency of the device is 403.55 MHz with transmission band of 402-405 MHz, which is the frequency range allocated on a shared basis for the US Medical Implant Communication System (MICS) FCC 47CFR Part 95.

This chapter focuses more on the sensor device. A short review of the base station will be covered in Appendix section. The cocaine detector consists of three main components. They are the active elements of the biosensor, the read-out electronics, and the compartment which holds both the active elements and the electronics. The biosensor active elements must form a the small, simple, inexpensive, yet sensitive sensor. Other requirements for the cocaine sensors include: low current consumption, capability of operation at supply voltages down to 3.0 V, maximum battery life, and minimum complexity. These requirements can be achieved by selecting the right electronic components for the sensor read-out.

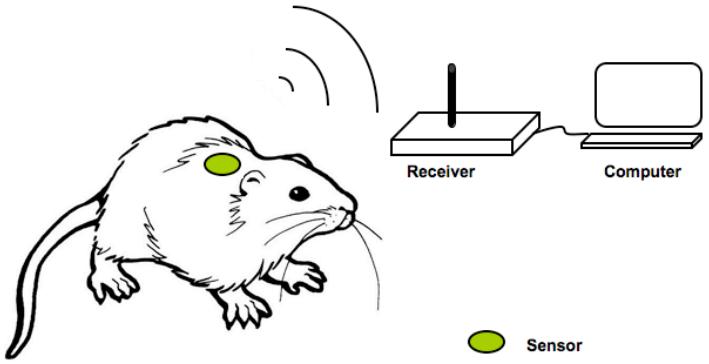

Figure 3.1: Conceptual drawing of implantable cocaine sensor system.

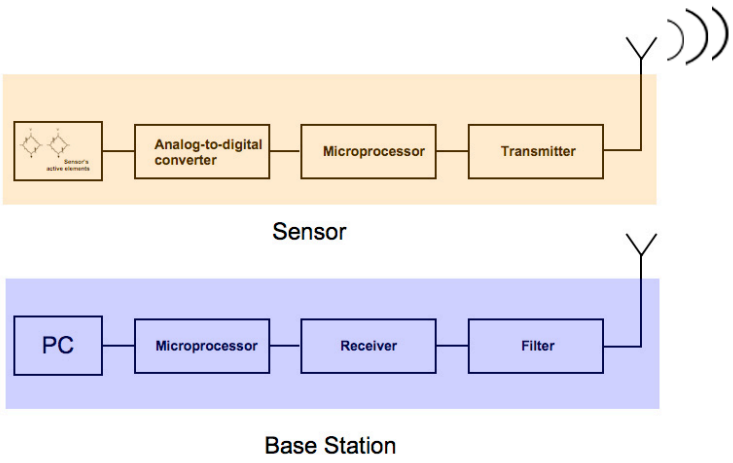

Figure 3.2: Block digram of the complete cocaine sensor system.

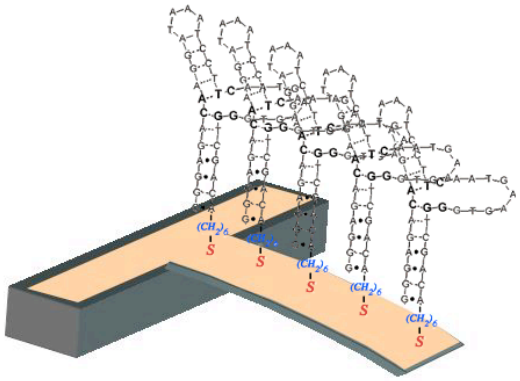

Figure 3.3: The active elements of the cocaine biosensor. It includes piezoresistive microcantilevers and an oligonucleotide–based aptamer as the cocaine binder.

3.1 The active elements

The active elements of the cocaine biosensor chosen in this work, as displayed in Fig. 3.3, are piezoresistive microcantilevers coated with oligonucleotide-based aptamer as the biological sensing element.

3.1.1 Oligonucleotide-based aptamer

Aptamers were chosen early in the project as a sensor coating due to their high selectivity. It is a new class of molecules that have recently been introduced as the rival to the antibody [13, 58]. An aptamer is an oligonucleotide sequence, a short sequence of RNA or DNA oligomers with a specific sequence of base pairs that form a highly selective three–dimensional structure with the capacity to recognize wide range of target molecules with high affinity and specificity. It can be used in therapeutic and diagnostic applications as well as a biological sensing element in biosensors. There are several reasons why aptamers are more promising for such applications in the future than antibodies. Antibodies are produced in animals, and identification and generation of antibodies depends only on the physiological conditions of the animals. The properties of the antibodies, such as the kinetic parameters of antibody-target interactions, are not easily altered. Their performance

can vary from batch to batch, requires optimizations for each batch and its applications. Storage is an additional challenge. Antibody-producing cells need to be frozen and stored at multiple sites to prevent death of cell lines. Furthermore, they have limited shelf life, are temperature sensitive, and can be irreversibly denaturated.

Aptamers, on the other hand, are produced *in vitro* by chemical synthesis, namely the SELEX (systematic evolution of ligands by exponential enrichment) process, in which a unique oligo (RNA/DNA) is identified or selected from RNA/DNA libraries containing random sequence oligomers. Example of such library is the Ellington lab aptamer database [59]. Aptamers properties can be customized or manipulated for enhanced stability, affinity, and specificity. There is little or no variation in performance from different batches. Moreover, they possess a high stability for long-term storage at ambient temperature and sustain reversible denaturation. An important quality of aptamers as biological sensing elements in biosensors is their ability to regenerate their function by varying heat, salt, concentration, pH, and addition of chelating agents. Integrated with specific transducers, aptamers can be use to detect different analytes or target molecules such as human Immunoglobin E (IgE) [60], the coagulation protein thrombin [61, 62], HIV-1 Tat protein which controls early phase of HIV-1 replication cycle [63], cancer-related proteins [64], and, of course, cocaine [16, 17]. More on aptamers development can be found in Ref. [59, 65].

The aptamer that is used as the cocaine receptor in the work has similar configuration as the aptamer **MNS-4.1** used in Ref. [16,17]. The difference lies in the addition of a thiol at the $5'$ end of the sequence which results in
`5'-(_C6Thiol)ACAGCTGGGTGAAGTAACTTCCTAAAAGGAACAGAGGG-3'`. Fig. 3.4 illustrates the aptamer's structure. In the absence of cocaine, the aptamer is a partially formed three-way junction. Cocaine binds to the aptamer through a hydrophic pocket located within the junction, causing the short stem to form and producing a fully defined three-way junction. Besides its low-micromolar dissociation constant ($\sim$ 0.4–10 μM), another advantageous feature of **MNS-4.1** aptamer is its selectivity for cocaine over cocaine metabolites.

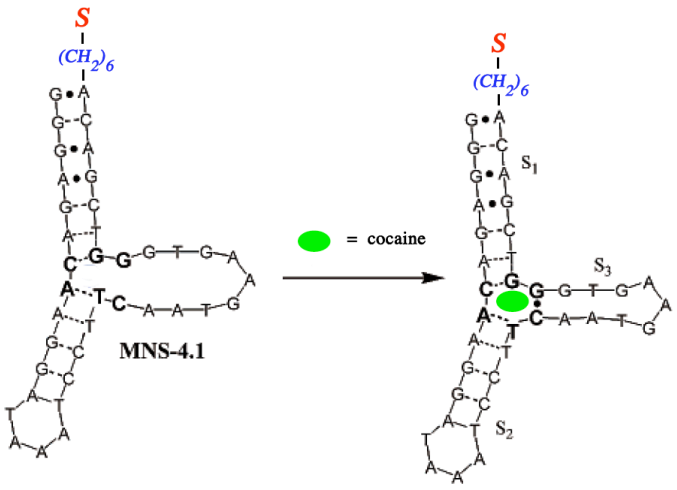

Figure 3.4: Structure of three-way junction of the aptamer used to bind cocaine adapted from Ref. [16, 17] with thiol at the 5′ end of the sequence.

The thiol attached to the 5′ end of the aptamer will help the immobilization process of the aptamer onto the gold-coated microcantilever surface (see Fig. 3.5). A thiol is an organic compound that has a thiol group, `(-SH)`. A strong, covalent-like bond between the sulfur and the gold atoms, which is on the order of approximately 50 kcal/mol [66], leads to chemisorption of the aptamer to the gold coated microcantilevers.

3.1.2 Piezoresistive microcantilevers

Piezoresistive microcantilever arrays manufactured by Cantion, Inc. are used as the sensor's transducer. Each array contains four piezoresistive microcantilevers which are fabricated with uniformly linearly doped (p-type) silicon "wires" encapsulated in Si_3N_4. The embedded 4 $K\Omega$ resistive wire is connected to two bond pads for each cantilever as shown in Fig. 3.6. Each array contains two bare Si_3N_4 cantilevers and two that are coated with 30 nm gold (Au) via a vacuum physical vapor deposition and with 2 nm chromium (Cr) as adhesion layer. Each rectangular-shaped microcantilever has dimensions of 50 μm width, 150 μm length, and 0.5 μm thick.

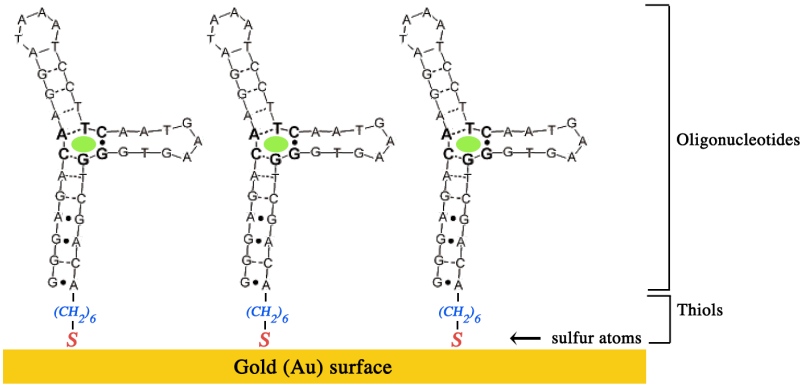

Figure 3.5: Immobilization of aptamer on gold surface via thiol.

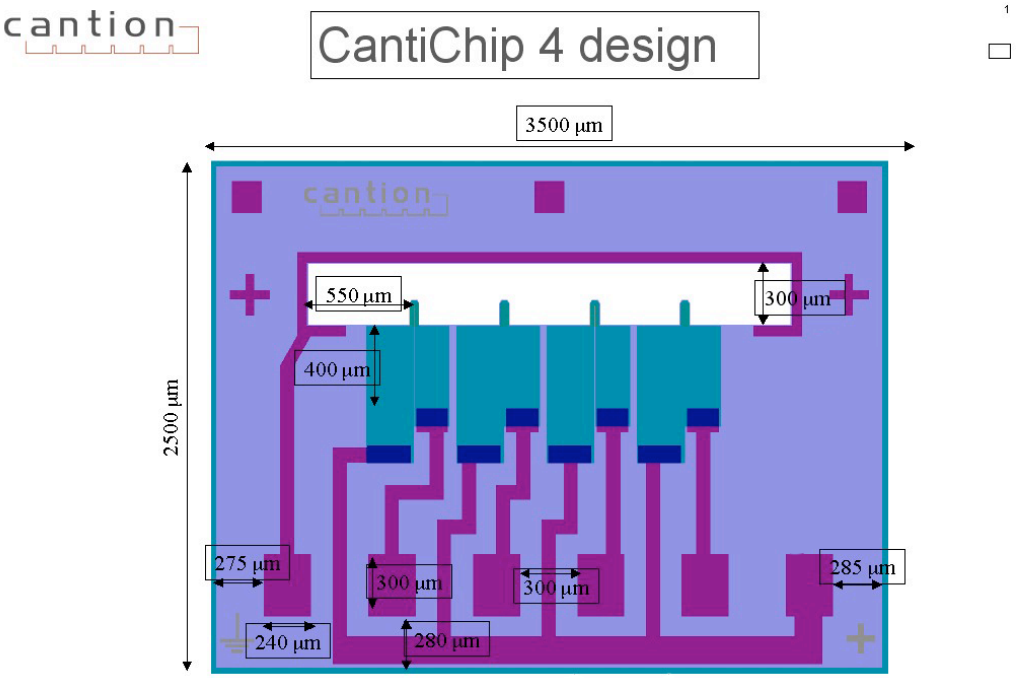

Figure 3.6: Schematic of Cantion piezoresistive microcantilever array.

A modified Wheatstone bridge, introduced by Tortonese [48] and mentioned in Chapter 2, is used to measure the cantilever deflection. In Tortonese's configuration, the bridge is made of three fixed-value resistors and one varying resistor originated from the piezoresistive microcantilever as shown in Fig. 3.7(a). The cocaine sensor's configuration uses four microcantilevers to form the bridge, two Si_3N_4 cantilevers and two gold-coated cantilevers whose resistance can be varied as illustrated in Fig. 3.7(b). The gold-coated microcantilevers are placed diagonally across from each other which proved to be the best configuration for our purposes. Here, the differential ouput voltage $(V_1 - V_2)$ is twice the value obtained with the original Tortonese's bridge, thus doubling the sensitivity of the sensor. In fact, the differential output voltage of the original Tortonese's Wheatstone bridge is:

$$V_o = V_2 - V_1 = V\frac{\Delta R}{4R} \tag{3.1}$$

In contrast, for the Wheatstone bridge with two varying resistance cantilevers that are diagonally across from each other, the obtained differential output voltage is:

$$\begin{aligned} V_1 &= V\frac{R}{R + (R + \Delta R)} && (3.2)\\ V_2 &= V\frac{R + \Delta R}{R + (R + \Delta R)} && (3.3)\\ V_o &= V_2 - V_1 = V\frac{\Delta R}{2R + \Delta R}, but \Delta R \ll R && (3.4)\\ &\approx V\frac{\Delta R}{2R} && (3.5) \end{aligned}$$

In other words, when the target molecules are captured on the functionalized gold-coated cantilevers surface, the resistance of the top left microcantilever increases, causing the output voltage, V_1, to decrease. At the same time, the resistance of the lower right microcantilever also increases, which leading to an increase in the output voltage, V_2. Both the decrease in V_1 and increase in V_2 result in increasing the differential output voltage, $V_2 - V_1$, of the diagonal-type Wheatstone bridge configuration.

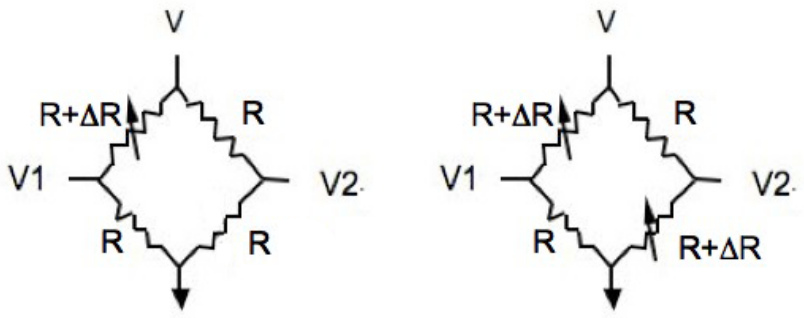

(a) (b)

Figure 3.7: Tortonese's vs. the cocaine sensor's Wheatstone bridge configuration.
(a) Tortonese's configuration with one varying resistor from piezoresistve microcantilever.
(b) The cocaine sensor's bridge configuration with two varying resistors diagonally across from each other.

Since one of the pads of each cantilever in the Cantion's array is tied to a common electrical connection as shown in Fig. 3.6, two arrays are required to build a Wheatstone bridge, where one gold-coated cantilever and one Si_3N_4 were selected from each array. Accordingly, two Wheatstone bridges can be built in a single device as described in Fig. 3.8.

3.2 Electronics Read-Out

The Wheatstone bridges data readings are controlled by the following electonic components:

(a) analog to digital converter

(b) microprocessor

(c) transmitter and antenna

These components are powered by two silver oxide batteries at 1.55 V each. Fig. 3.9 is the block diagram for the cocaine biosensor read-out.

3.2.1 Analog-to-Digital Converter

Analog to digital conversion is performed using the AD7792 chip from Analog Devices, Inc. chosen for its low power consumption, low noise on–chip instrumentation amplifier, output update rate options, on–chip digital filters, and a 16–bit sigma-delta ($\Sigma-\Delta$) modulator. The

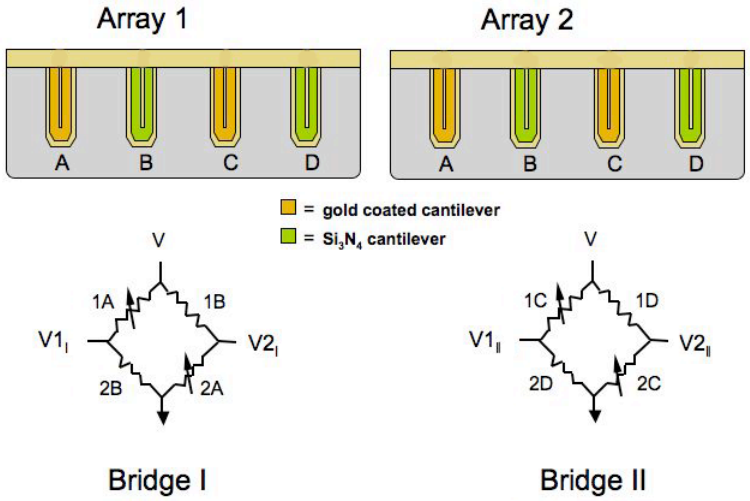

Figure 3.8: Microcantilevers arrangement in the sensor's Wheatstone bridges.

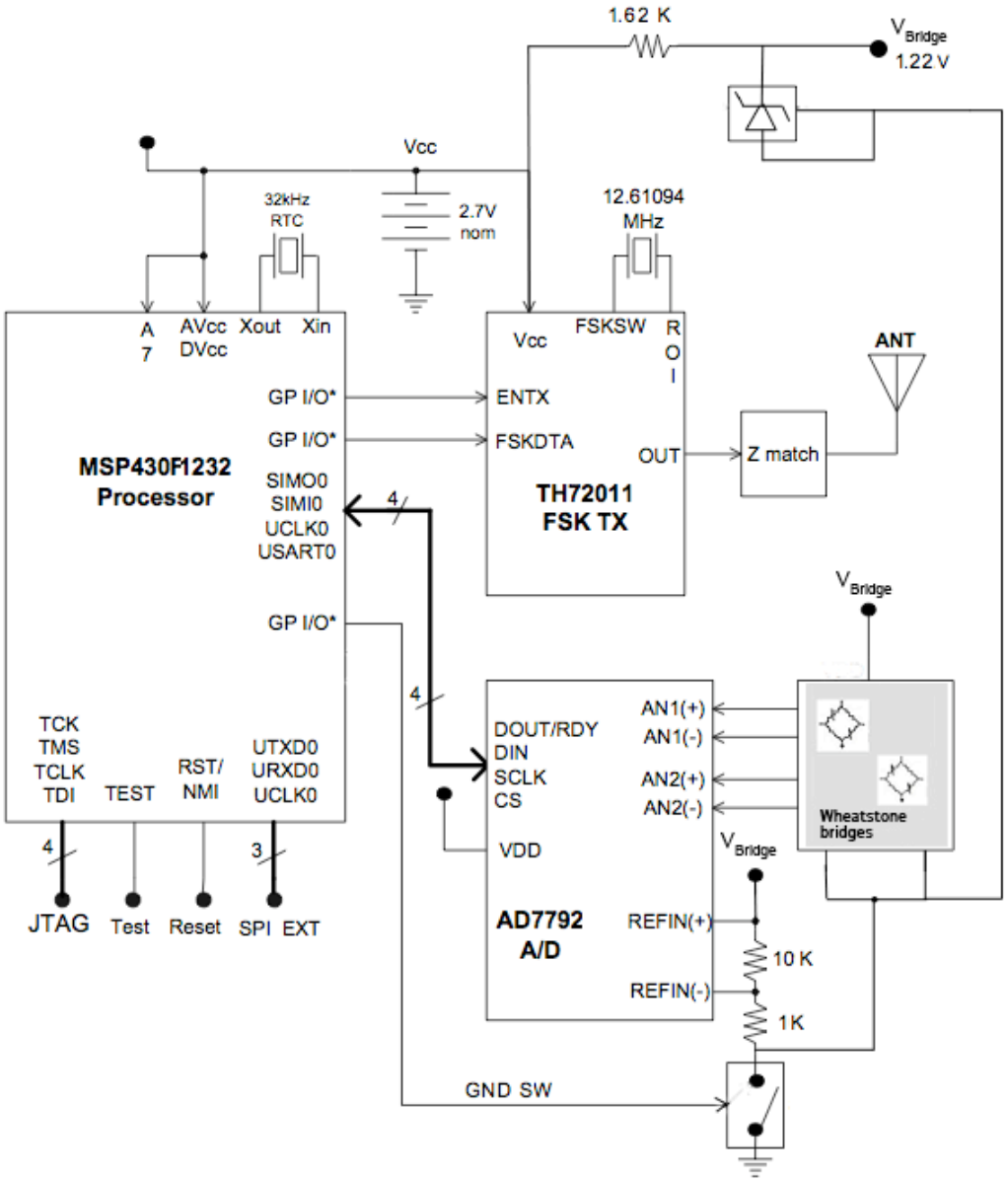

Figure 3.9: Block diagram of the cocaine biosensor electronics read out.

device's operating voltage ranges from 2.7 volts to 5.25 volts with 400 μA typical current consumption. The on–chip instrumentation amplifier or *in–amp* allows small amplitude signal to be interfaced directly to the device. The amplification factor can be achieved by setting a gain of 1, 2, 4, 8, 16, 32, 64, or 128 that may be selected by programming specific bits in the device's configuration registers. The digital output update rate, which is also user–programmable, ranges from 4.17 Hz to 470 Hz. The chip uses different types of digital filters depending on the update rate. A simultaneous 50 Hz and 60 Hz rejection is optimized when the update rate is 16.7 Hz or less, within which the rate used by the cocaine sensor is.

The analog to digital conversion in the AD7792 is accomplished using a $\Sigma-\Delta$ modulation method. A brief overview of the modulation method is as follows, according to Ref. [67]. As demonstrated in Fig. 3.10, an analog input voltage is added to the output of the feedback from a digital-to-analog converter (DAC) which is 0 V at initial condition. The result is passed into an integrator where it is added to a value from previous integration whose initial value is also 0 V. A comparator then checks the output of the integrator: if it is greater than or equal to zero volts, then a logic 1 is sent out, otherwise a logic 0 is sent out. The bit is fed to a DAC node. In the DAC node, the DAC sends out +VREF voltage to the summing node when it receives logic 1 from the comparator, or -VREF when it receives logic 0. The output bit from the comparator is also sent to a digital filter before being delivered in a serial data stream. The advantage of the delta-sigma modulator for the the sensor application is its very high resolution digital output due to oversampling of the analog input.

A battery is connected directly V_{DD}. Pin AIN(+) and AIN(-) receive signals from the differential voltages of the Wheatstone bridge in the sensor, V_2 and V_1 respectively. The reference voltage of the device is supplied by a 1.22 V external voltage reference. The serial clock input, SCLK, which is set to noncontinous mode for the application, is regulated by a the microprocessor which will be covered in the next subsection. The AD7792's data input, DIN, carries bits information from the microprocessor to the ADC shift registers. This information sets the values of the appropriate registers within the ADC to certain values.

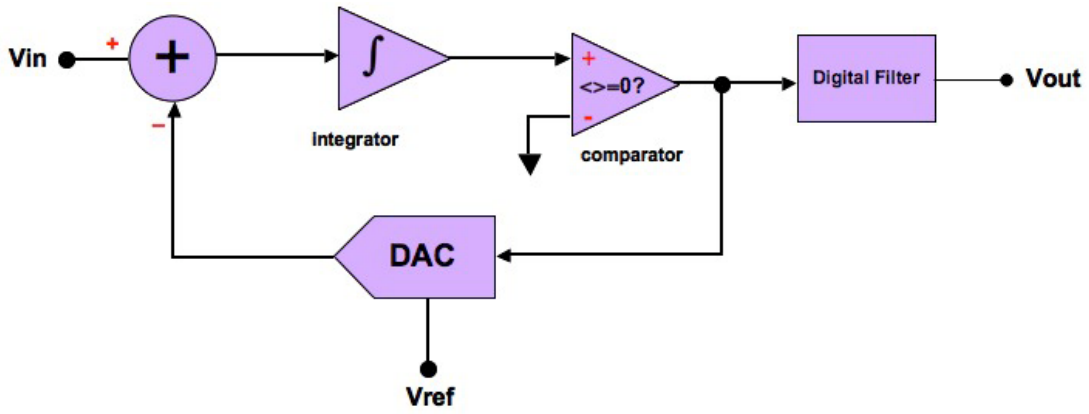

Figure 3.10: Flow chart of Sigma-Delta ($\Sigma - \Delta$) modulation [67].

The serial data output/data ready pin, DOUT/$\overline{RDY}$, has dual functions. As DOUT, it transfers serial data stream from the ADC to the microprocessor. As data ready pin, it is an indicator whether the data conversion from analog to digital has been completed.

3.2.2 Microprocessor

The microprocessor used in the sensor needs to performed the following tasks:

(a) All system timing, including real time clock generation

(b) Battery status monitoring and management

(c) MEMS A/D control for temperature sensor

(d) Data packet formation and transmission

The MSP430F1232 manufactured by Texas Instruments, Inc. meets the above requirements for several reasons. First, the microprocessor has low operating voltage, ranging from 1.8 V to 3.6 V, and a very low current consumption, 0.7 μA in standby mode and 200 μA in active mode. This low power consumption is very significant to achieve extended battery life in portable measurement applications such as the present cocaine sensor. Another important feature of this device is that it allows fast switching, less than 6 μs, from a low-power mode or standby mode to an active mode. This feature helps the sensor in optimizing the battery life. Despite its small package size (5mm x 5mm), the microprocessor has sufficient memory capacity of 8KB + 256B flash and 256B RAM. It is also equipped with a built-in

real time clock (RTC), internal A/D used by the sensor for battery voltage monitoring and a temperature sensor, and twenty-two general purpose input/output (GPIO) pins.

The processor is powered by the sensor battery. As shown in Fig. 3.9, the battery is also input to the pin A7 for voltage monitoring. The system real-time clock is generated by using a 32.768 KHz watch crystal oscillator, connected to pins XIN and XOUT.

The microprocessor operates in two modes: sleep mode and normal or active mode. Referring to Fig. 3.11, in the sleep mode, the GND SW signal out is low, leaving the FET switch open. Since there is no current flow, the input voltage across the Wheatstone bridge is zero, and accordingly, the bridge's differential output voltage is zero. The typical current consumption in the sleep mode is approximately 2 μA for operation at 1 MHz. This is the lowest power mode provided by the device which still allows the CPU to wake up. The active mode includes powering up the sensor bridges, reading the values from the ADC via the general purpose I/O pins, constructing data packet in RAM, and transmitting the data packet to the transmitter chip via other GPIO pins. In this mode, the GND SW signal out is set to high, causing the FET switch to close and creating a current path from the voltage source to the ground. This allows the external reference voltage to power up the Wheatstone bridge. This value is the highest voltage that is allowed to prevent the cantilevers from overheating.

The interval time between the sleep and active modes is currently set to 8 seconds. This value can be reconfigured via the watchdog timer feature of the microprocessor. The data packet contains time stamps, the sensor identification, battery status, packet number, sensor temperature, current measurements from bridge I and from bridge II, previous measurements from bridge I and from bridge II, parity bits, and data error checking using Cyclic Reduncancy Code (CRC) as listed in Table 3.1. The packet is then delivered to the RF transmitter using Manchester encoding.

Manchester encoding is done by representing one bit with a high-to-low or low-to-high transition in the midpoint of the bit period. The binary **1** is set by setting the voltage high at the first-half interval of the bit period and voltage low at the second-half interval.

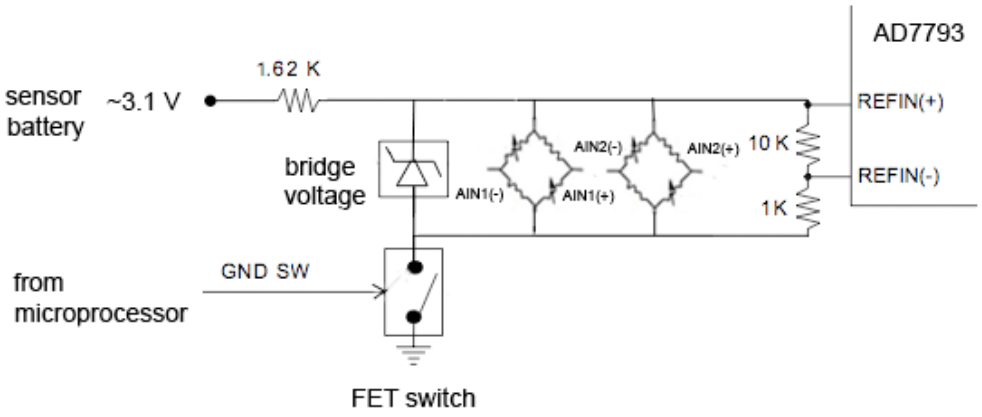

Figure 3.11: Part of the sensor's schematic diagram which shows the FET switch that is controlled by the microprocessor modes. In sleep mode, the FET switch is open, no current flows. In active mode, the FET switch is closed, powering the sensor's bridges.

Table 3.1: Content of sensor transmission packet.

Field	**Size (bits)**	**Bit position***	**Description**
Run-in	16	b0–b15	AAAAh. Used for receiver bit synchronization
Start inicator	16	b16–b41	D4D4h. Used for receiver packet synchronization and marks the start data
Status	6	b42–b47	Sensor status. See 3.2
Count	10	b48–b67	Count calue of Measurement Counter, incremented each transmission
Temperature	8	b68–b75	Sensor temperature measurement
ID (upper 8 bits)	8	b76–b93	High byte of sensor identifier
ID (lower 16 bits)	16	b94–b119	Lower 2 bytes of sensor identifier
MEMS–I	16	b120–b145	Measurement for MEMS bridge I
MEMS–II	16	b146–b171	Measurement for MEMS bridge II
PREV MEMS–I	16	b172–b197	Previous measurement for MEMS bridge I
PREV MEMS–II	16	b198–b223	Previous measurement for MEMS bridge II
CRC	16	b224–b249	CRC for data error check.

Table 3.2: Sensor status bits.

Bit	**Indication (bit=1)**
b42	reserved
b43	reserved
b44	reserved
b45	Sensor operation error
b46	Sensor measurement error
b47	Low battery

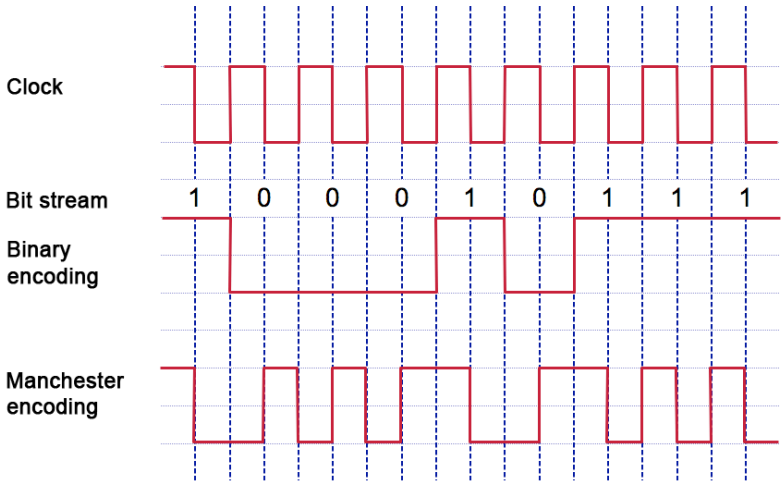

Figure 3.12: Manchester encoding of a given bit stream adapted from Ref. [68].

The opposite applies to the binary **0** where voltage low occurs at the first-half and voltage high at the second-half interval. The Manchester encoding is shown in Fig. 3.12. The advantage of this encoding scheme with transition in the middle of bit period is to permits synchronization between the transmitter and receiver [68]. Furthermore, the clock frequency and synchronization information are embedded in encoded data.

3.2.3 Transmitter and Antenna

To transmit the encoded sensor data to the base station, the TH72011 transmitter chip manufactured by Melexis, Inc. is selected. The transmitter is compatible with the Europian industrial-scientific-medical (ISM) band at 433 MHz, but it also provides broader frequency range from 380 MHz to 450 MHz. To meet the nominal center frequency of 403.55MHz required by the US Medical Implant Communication System (MICS), a 12.6109 MHz reference crystal is utilized as shown in Fig. 3.9. The value of the reference frequency derives from the formula given in the device's specification sheet: $f_{ref} = f_c/32$, where f_c is the carrier frequency which is 403.55 MHz. The block diagram of the transmitter is described in Fig. 3.13.

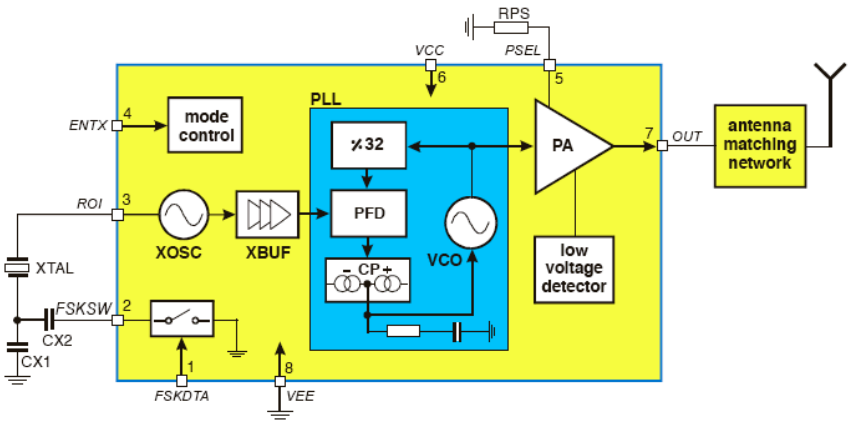

Figure 3.13: Transmitter chip TH72011 block diagram [69].

The frequency-shift keying (FSK) modulation method is used to transmit the data packet as demonstrated in Fig. 3.14. The data are transmitted by using different carrier frequencies: the logic **0** is transmitted at frequency f_{c0} and the logic **1** at frequency ω_{c1}. The carrier frequencies for FSK low (**0**) and FSK high (**1**) are defined from the the lowest and highest frequency range allowed by MICS. The FSK scheme is selected due to its low power and better noise immunity than other modulation schemes. The modulated data packet is then transmitted to the receiver via two loop antennas which are placed around the sensor's printed circuit board. Passive components to be selected are used to optimize impedance matching thus minimizing losses.

3.3 Sensor Encapsulation

The piezoresistive microcantilever arrays and the electronic components are laid on two PC boards: the upper and lower boards as described in Fig. 3.15. The upper printed circuit board contains the two turns of the loop antenna, one on each side of the board. The lower PC boards contain microcantilevers arrays, refers as MEMS in the figure, and the rest of the electronic components. Spacers are placed between the upper and the lower boards to avoid contact between the boards and to give enough room for two stacked batteries which are placed at the end of the boards and secured by a pair of metal tabs.

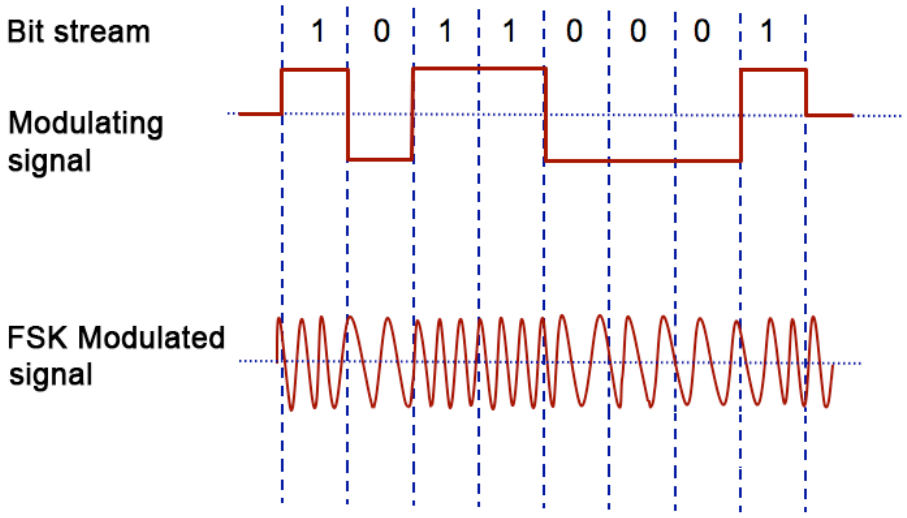

Figure 3.14: FSK modulation [70].

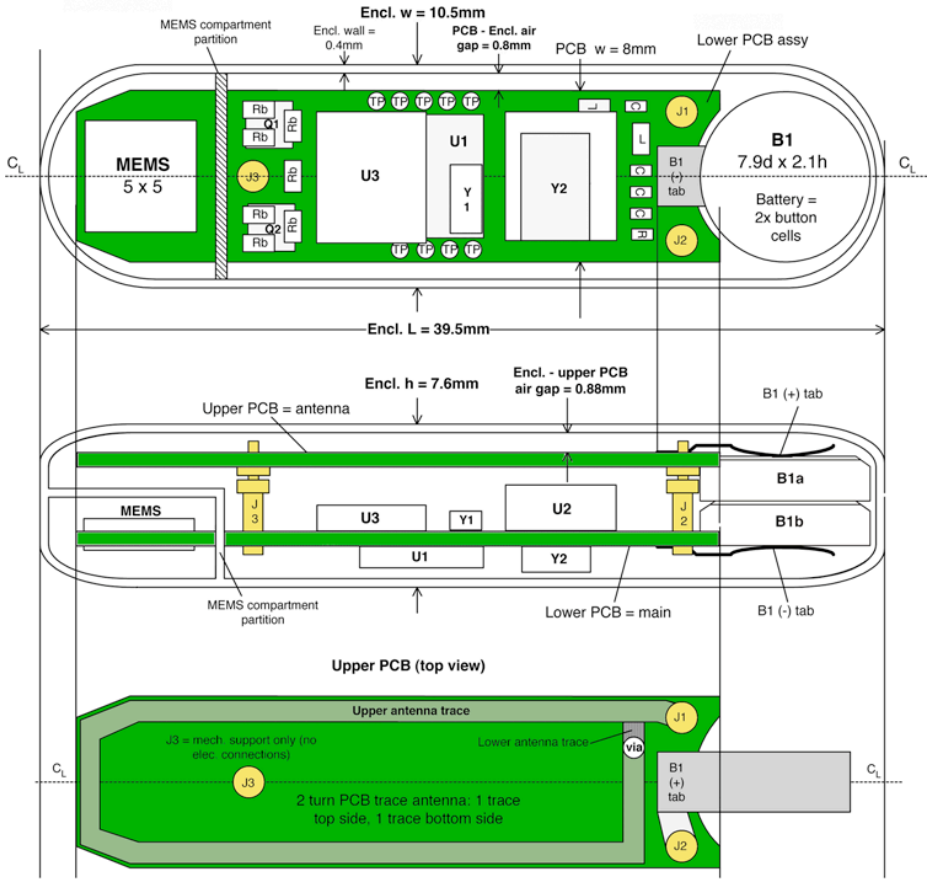

U1 - microprocessor
U2 - transmitter chip
U3 - ADC

Y1 - 32.68 KHz crystal
Y2 - 12.61 KHz crystal

J1, J2, J3 - spacers
TPs - test points

Figure 3.15: The sensor's PC layout.

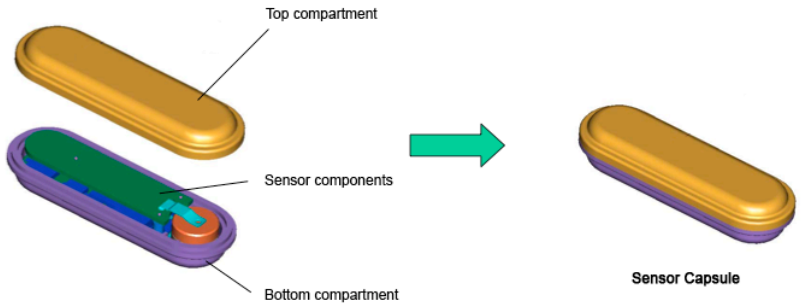

Figure 3.16: The sensor compartment is made up by the top and bottom housings.

The sensor is placed in a compartment or a housing. The challenge in choosing and designing the compartment lies on the biocompatibility of the compartment material and the ability to provide a water tight seal between electronic components and the sensor environment but leaving the active elements, i.e. the aptamer-coated microcantilever arrays, exposed to the interstitial fluid. A thermoplastic polyetherimide high heat polymer, Ultem–1000, is selected for the housing material due to its high strength and high heat resistance which provide flexibility during molding to obtain a preferred shape of the capsule and which allow autoclave sterilization [71]. The material is FDA and USP (U.S. Pharmacoepia) class VI compliant.

The housing is formed such that there are no sharp edges or features on the external part of the housing that could possibly interfere with the implantation. As demonstrated in Fig. 3.16, the compartment is divided into two parts, top and bottom housings, to give an easy access to insert and replace the sensor boards as well as the batteries, with the lower printed circuit board fit well in the bottom housing. The bottom housing contains a small window as displayed Fig. 3.17. The window, which is positioned below the microcantilever arrays, will allow interstitial fluid to flow to the sensor active elements. A ring of double-sided polyester tape, Tesa-4967, is placed around the small window on the inside part of the housing. As shown in Fig. 3.15 this tape ring forms a seal to isolate the electronic components from the fluid. Fig. 3.18 demonstrates a complete assembly of the sensor capsule.

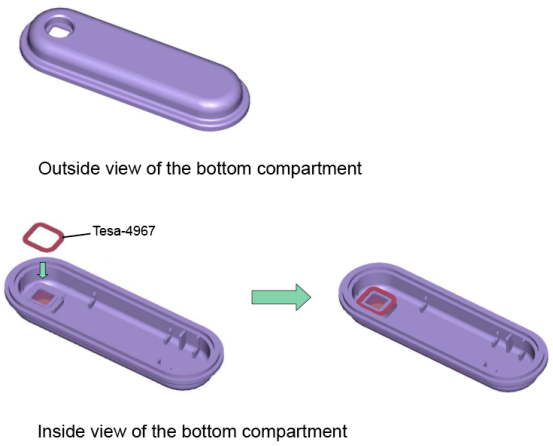

Figure 3.17: The bottom compartment of the sensor contains a small window that allows interstitial fluid to flow to the microcantilever arrays.

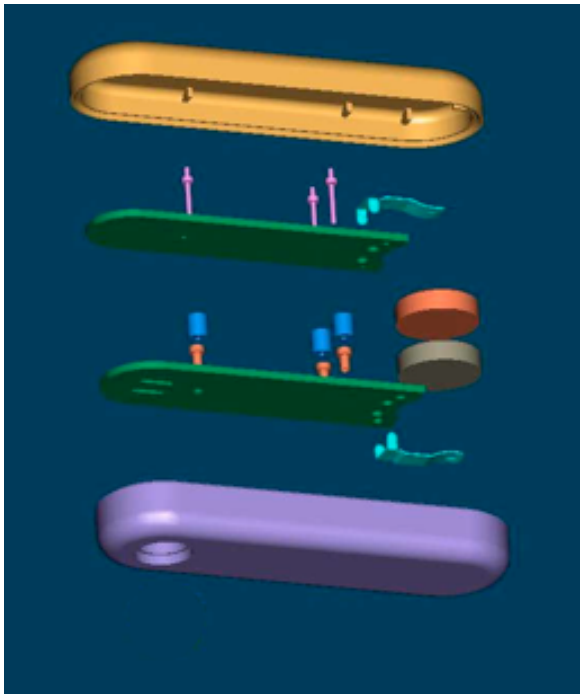

Figure 3.18: Illustration of sensor capsule assembly.

Chapter 4

Experimental Setup

4.1 Immobilization of aptamer

Before modifying the gold coated microcantilevers, an attachment test of aptamer is done on a bigger surface for optimization of the immobilization process. A quartz crystal microbalance (QCM) is chosen for this purpose because the QCM provides information how much aptamer covers the gold surface.

Quartz crystal microbalance.

Quartz crystal microbalance (QCM) consists of a thin quartz crystal disk sandwiched by electrodes as shown in Fig. 4.1. The crystal itself is a piezoelectric material. When an external electrical potential is applied across the crystal, it generates an internal mechanical stress [72]. The crystal is integrated into an oscillation circuit at resonant frequency near its fundamental frequency. The fundamental frequency depends on the crystal's thickness, chemical structure, shape, and mass. The resonant frequency, however, can be changed when additional mass is applied on the crystal. The Sauerbrey equation (Eq. 4.1) shows the change in resonant frequency, Δf, due to change of mass, Δm, is given by [73, 74]:

$$\Delta f = -C_f \cdot \Delta m \tag{4.1}$$

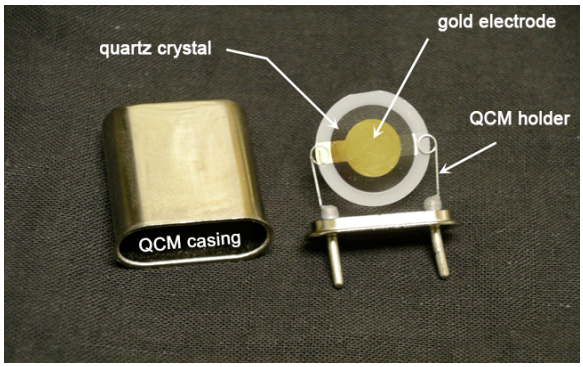

Figure 4.1: A quartz crystal microbalance (QCM).

where C_f is the sensitivity factor of the crystal. A typical value for a 5 MHz AT-cut quartz crystal at room temperature is 56.6 Hz $\mu g^{-1} cm^2$. The equation implies that the amount of added or reduced mass to the crystal can be determined by measuring the shift in its resonant frequency.

QCMs have been used widely used in thin film deposition. However, recently they have been applied more for analysis tools as gas phase detectors for organic vapors e.g. toluene, benzene, heptane, and xylene [75, 76] and for environmental pollutants [77, 78], and as immunosensors to identify various analytes such as pesticides [79], bacteria [80–82], and viruses [83, 84]. Other applications are DNA biosensors to detect DNA hybridization [85–87] and drug analysis [19, 88, 89].

Aptamer preparation

The oligonucleotide-based aptamer that is used to bind with cocaine is manufactured in the laboratories of The Midland Certified Reagent Company (Midland, TX) and has been purified from any extraneous salt by gel filtration chromatography (GF grade). The quantity of the material is given in nanomoles and in A260 units, with A260 refers to the absorption wavelength of the aptamer. One A260 unit equivalent to 30–35 micrograms of DNA. The sequence of the aptamer and the placement of the thiol group at the $5'$ end of the sequence is mentioned in Chapter 3. Since the sulfur in the thiol group is very reactive, the aptamer is received with a trityl protecting group attached to the sulfur and it is in a lyophilized

(freeze-dried) form. Certain procedure to resuspend and to free the thiol group before using the aptamer can be found at the company's website [90]. Details on the procedure that has been customized for the aptamer is listed in Appendix. When it is not being used, the free thiol aptamer solution is stored under an inert atmosphere and placed in -20^{o}C, which gives a shelf life between 6 weeks to a year. A Cary 50 UV-Vis spectrophotometer is used to read the aptamer spectrum to verify that the aptamer still presents after the deprotecting process.

Immobilization process

The aptamer is thiolated at one end so that it can be thethered to a gold film on a sensor due to the affinity of the sulfur in the thiol for the gold. It was not clear initially, that the stereochemistry allowing unique binding in a solution would also prevail in the case that one end of the aptamer is bound to a surface and surrounded by similarly bound aptamers. Therefore, the initial experiments required studies of the binding as determined using a quartz crystal microbalance.

Prior to attaching the thiol group to its gold surface, the QCM is cleaned by rinsing it with acetone, isopropanol, and ethanol, consecutively, followed by drying it with N_2. The crystal is submerged in the aptamer solution and placed in -4^{o}C storage room. Immersion time is varied to obtain maximum aptamer coverage. After the specified amount of immersion time, the QCM is removed from the aptamer solution, rinsed in distilled water to wash away any contamination, and dried using N_2 stream.

Measurement setup

To determine the amount of aptamer that is attached to the gold surface of the QCM, the resonant frequency of the crystal is measured before and after aptamer adsorption. Fig. 4.2 describes the measurement setup. A QCM with resonant frequency 6.00 MHz is purchased from the International Crystal Manufacturing Co, Inc. (Oklahoma City, OK) [91]. The crystal has a diameter of 13.66 mm and is coated in the central 6.8 mm in diameter with

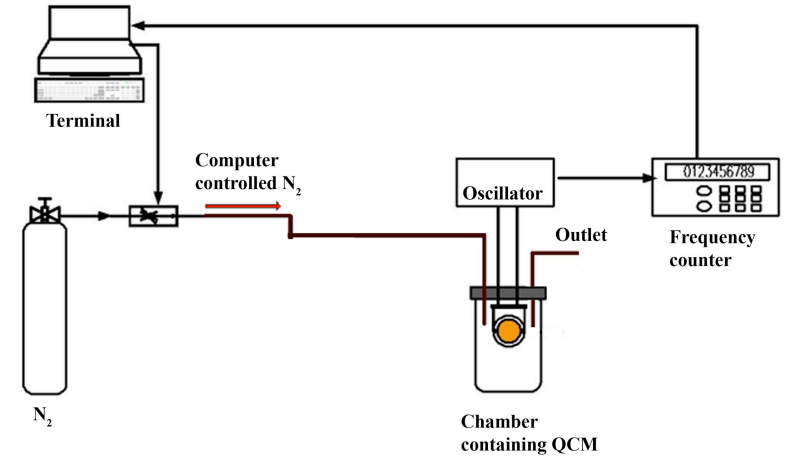

Figure 4.2: Experimental setup to measure resonant frequency of the QCM.

100 nm of polished gold on both sides using 10 nm of titanium as the adhesion layer underneath the gold. The QCM sensor is placed inside a 35 mm diameter glass bottle. The QCM is driven by a 6.0 MHz oscillator which is also obtained from the International Crystal Manufacturing Co, Inc. Two tubes are inserted into the bottle, one for the vapor inlet and the other for the outlet. Nitrogen gas is streamed into the bottle to eliminate water vapor and to keep a contant relative humidity. The flow rate of the N_2 is set to 100 sccm (standard cubic centimeters per minute), and is controlled by an MKS Mass-Flo Controller (MFC) 1479A from MKS Instruments. Changes in the resonant frequency of the QCM are recorded using an Agilent 53131A 225MHz universal counter.

4.2 Relative cocaine concentration measurement using quartz crystal microbalance

A quartz crystal microbalance is also used to detect cocaine. Once the gold electrodes of the QCM have been modified with the aptamer, a 'dip and dry' [79, 84] method is conducted to observe any cocaine that binds onto the crystal. This method is carried out by dipping the aptamer-functionalized QCM into the cocaine solution for a specified amount of time, rinsing it in distilled water, and then drying it with N_2 stream. The resonant frequency of

the crystal is measured before and after cocaine immersion. The same experimental setup as shown in Fig. 4.2 is used.

4.3 In vitro cocaine detection using piezoresistive microcantilever in a flow controlled system

In a flowing solution, the sensor is placed such that cocaine solution flows over the microcantilever arrays. The experiment is done for both wired and wireless sensors. The wired sensor, where the sensor is physically connected to a computer for signal reading, is intended to make sure that the sensor's active elements perform as expected before integrating them with the electronic components. It is the simple version of the implantable cocaine biosensor.

4.3.1 In vitro relative cocaine concentration measurement in a flow controlled system using the wired sensor

In this experiment, the prototype of the implantable cocaine sensor with a simplified version printed circuit board is presented. Each microcantilever array purchased from the Cantion is mounted on a green printed circuit board as shown in Fig. 4.3. Two arrays are needed to build a Wheatstone bridge. The bridge is connected to another printed circuit board that contains an analog to digital converter AD7793 from Analog Devices which also uses a sigma–delta modulator as in AD7792 but with 24–bit resolution instead of 16 bits. Here the differential bridge voltage as a function of cantilever resistance may be converted to a serial data stream. A USB data aquisition board is used to interface the digital signal to the computer. Power to the sensor's electronic components is supplied by the USB connection to the computer. Therefore, no external battery and no optimization of battery life are required. To create a flow, a channel is built over the microcantilevers arrays – refer to Fig. 4.3(b) – such that the solution flows in a transversal direction of the cantilevers. The channel sides are created using double sided foam tape on the printed circuit board with

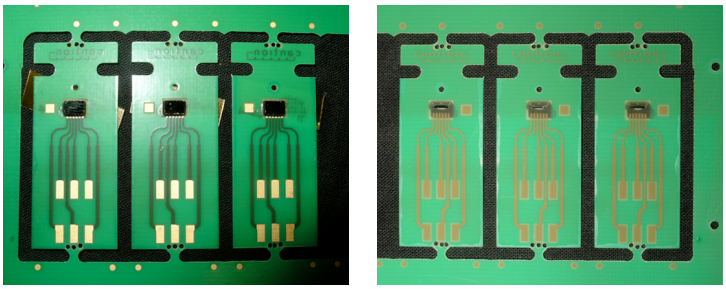

(a) (b)

Figure 4.3: Cantion microcantilever arrays mounted on a printed circuit board. (a) Microcantilevers facing down. (b) Microcantilevers facing up – the side where the flow channel will be fabricated.

the microcantilevers are facing up. A microscope slide with thickness of 0.13 – 0.17 mm is used to cover the channel to prevent overflow yet still be able to observe the solution flow. Detail on the fabrication process can be found in the Appendix. Fig. 4.4 show the device used in this experiment.

The experimental setup of the wired cocaine sensor is described in Fig. 4.5(a). The flow channel is connected to a six-port valve with 1-ml loop, a syringe pump, and two syringes. One syringe (A) is placed on top of one inlet port of the valve, and the other syringe (B) is connected to the bottom port and is driven by a pump. The six-port valve runs in two modes: LOAD and INJECT. In the load mode, illustrated in Fig. 4.5(b), the solution in the syringe B flows directly into the channel. In the inject mode, solution in syringe B pushes a solution that is in the 1-ml loop into the channel. For example, if syringe A solution has previously filled the loop, the syringe B solution will push solution A into the channel.

The flow system is controlled using two LABVIEW-based user interface programs. The first one is a syringe pump controller as displayed in Fig. 4.6. The program requires inputs from the users such as the syringe diameter, pumping direction, maximum volume to be delivered, and the most important input is the flow rate. As the feedback, the syringe pump controller displays the amount of liquid being pumped to the flow system.

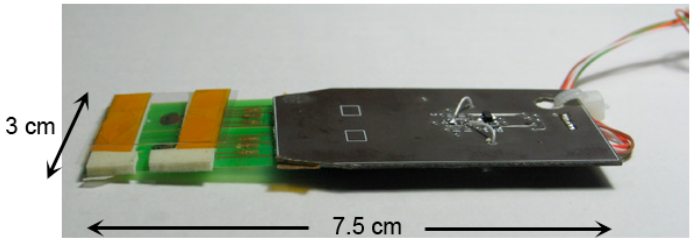

(a)

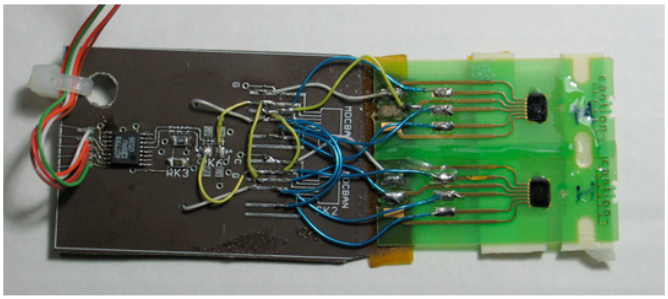

(b)

Figure 4.4: Wired sensor used in a flow controlled system. (a) Side view. (b) Top view.

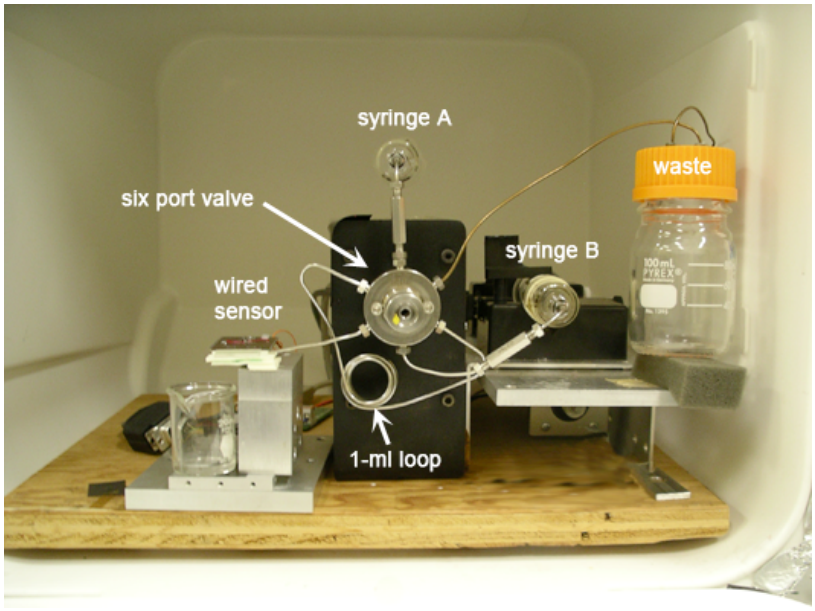

(a)

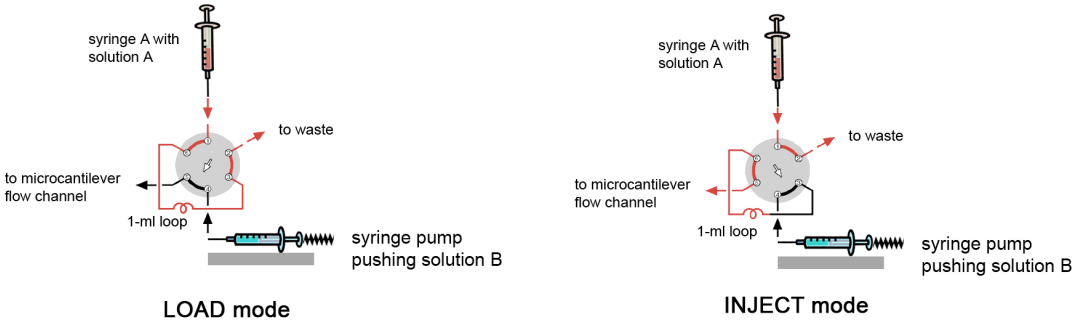

(b)

Figure 4.5: Experimental setup of the wired cocaine sensor in a flowing solution. (a) Photo of the experimental setup. (b) Two modes of the six-port valve.

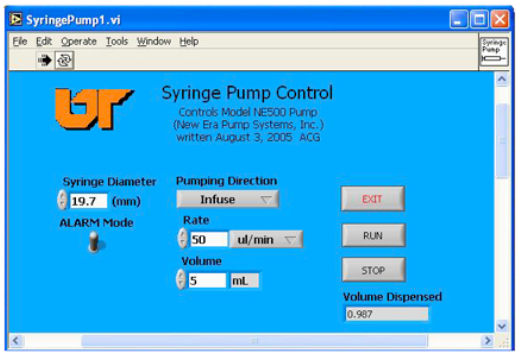

Figure 4.6: Graphical user interface of the syringe pump controller.

The other program, shown in Fig. 4.7, functions as data acquisition, which serves as an interface between the Wheatstone bridge and the AD7793. It allows users to set certain parameters such as the AD7793 gain, data update rate, and voltage reference, and to check the voltage of the power supply. The program's display window provides the users with a tool to monitor the signals of both the Wheatstone bridges.

4.3.2 In vitro relative cocaine concentration measurement in a flow controlled system using the wireless sensor

The purpose of this experiment is to verify the performance of the electronic components of the wireless sensor. The same circuit board and the electronic components described in Chapter 3 is utilized. The microcantilever arrays that are originally attached to the board were replaced by soldering the the Cantion arrays (Fig. 4.3) on the printed circuit board to allow fabrication of a flow channel as described in subsection 4.3.1. The modified wireless sensor for the flow controlled system is shown in Fig. 4.8. The wireless sensor and the flow channel are then attached to six-port valve as previously shown in Fig. 4.5. The same experiment procedures as in the wired sensor is carried out with the output signals from the bridges are expected to be similar also, except that the update rate in the wireless sensor is programmed to be slower compared to that in the wired sensor to maximized the battery life.

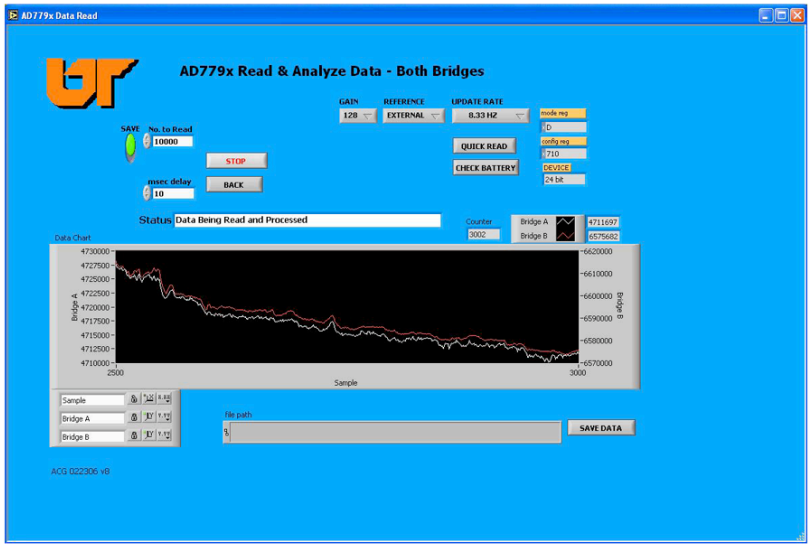

Figure 4.7: Graphical user interface of the data acquisition program for the wired sensor.

The graphical user interface for the wireless sensor data acquisition is different from that of the wired sensor. The GUI is presented in Fig. 4.9. It shows that it is able to read output signal up to six sensors distinguished by their ID numbers. Users do not have to enter any input since the parameters needed has been programmed in the MSP430f1232 microprocessor. In addition to showing the sensor output signal, the program also displays the battery voltage, the sensor temperature, the expected and actual number of packets received by the receiver, and the quality of the signal received for particular sensor.

4.4 In vitro relative cocaine concentration measurement using piezoresistive microcantilever in a stagnant solution

The experiment relies on diffusion of cocaine solution in distilled water which mimics the mechanism of the sensor when it is implanted in the body. The sensor capsule is placed in a petridish. The petridish is filled with distilled water that is enough to submerge the capsule. After the signal from the sensor is stabilized, a cocaine solution is introduced into

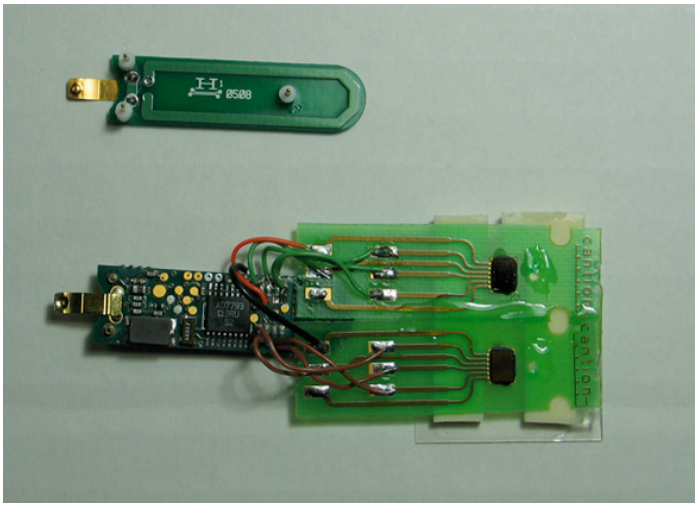

Figure 4.8: Wired sensor used in a flow controlled system.

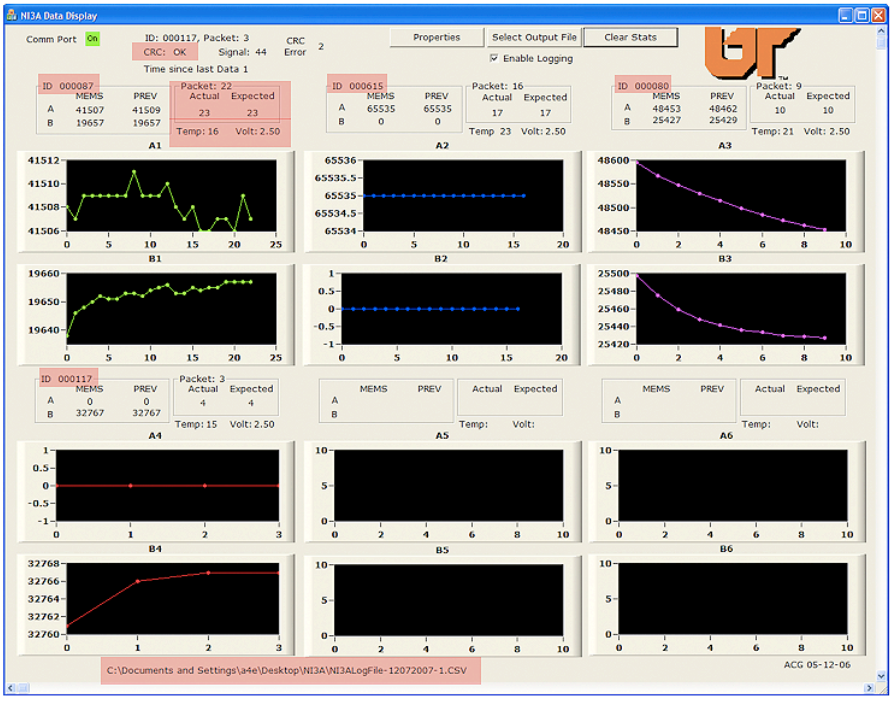

Figure 4.9: Graphical user interface of the data acquisition program for the wireless sensor.

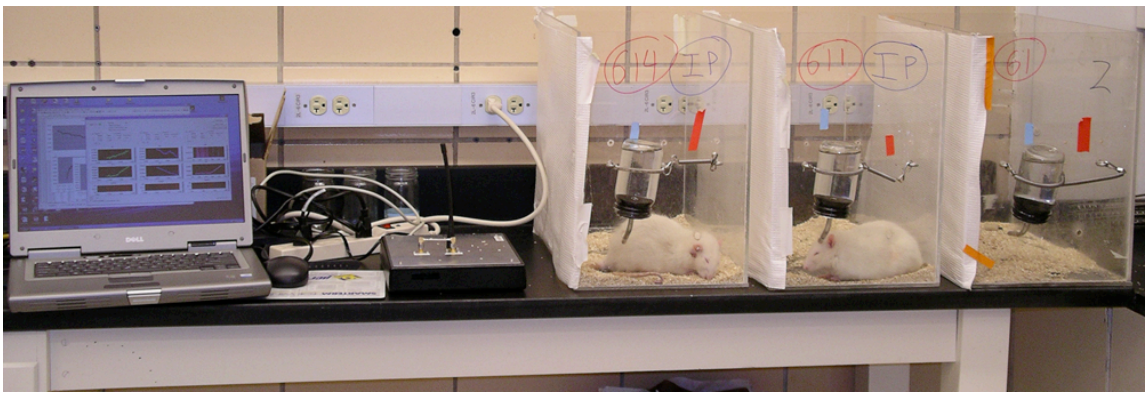

Figure 4.10: Experimental setup of in vivo cocaine detection in Wistar rats.

the water using a pipette. Since the signal is transmitted wireless, the same data acquisition program as previously shown in Fig. 4.9 was utilized.

4.5 In vivo cocaine detection in Wistar rats

The sensor capsule was taken to Indiana University Purdue University at Indianapolis (IUPUI) where it was surgically implanted under the skin at the nape of a male outbred Wistar rat. Animals used in this study are maintained in facilities fully accredited by the Association for the Assessment and Accreditation of Laboratory Animal Care (AAALAC). All research protocols are approved by the Institutional Animal Care and Use Committee and are in accordance with the guidelines of the Institutional Care and Use Committee of the National Institute on Drug Abuse, NIH, and the Guide for the Care and Use of Laboratory Animals of the National Research Council, 1996. The Wistar rat was implanted with the sensor and after a surgical recovery period, the sensor signal was monitored. Once stabilization is achieved, the rat was given an IP injection at certain dose depending on the mass of the rat. The injection may be repeated after the signal is settled again. Fig. 4.10 displays the experimental setup of the in vivo test. It consists of sensor-implanted rats, a base station, and a computer for data display and data acquisition.

Chapter 5

Results and Discussion

5.1 Immobilization of aptamer

5.1.1 Aptamer preparation

From the deprotecting process of lyophilized oligonucleotide, the obtained concentration of the thiol-free aptamer is 90.85 μM. Fig. 5.1 shows the UV-Vis spectrophotometer reading of the aptamer spectrum with absorption peak near 260 nm wavelength as expected. Another peak at 223 nm can be originated from other molecule structures contained in the aptamer, such as the thiol group which achors the aptamer to the gold surface.

5.1.2 Aptamer immobilization on QCM

As mention in Chapter 4, the immersion time of a clean QCM in the aptamer solution is varied to find the optimal time which maximizes the aptamer coverage on the gold surfaces. It started with an overnight immersion. This is based on Ref. [66] that suggests ∼12–18 hours immersion at room temperature to form self-assembly monololayers (SAMs) of thiols in ethanolic solution at concentration of ∼1–10 mM. The immersion time was increased from several days to a week based on the following experimental conditions which affect the adsorption of the molecules on the gold substrate: concentration, temperature, and solvent. The temperature at which the immersion takes place influences the kinetics of

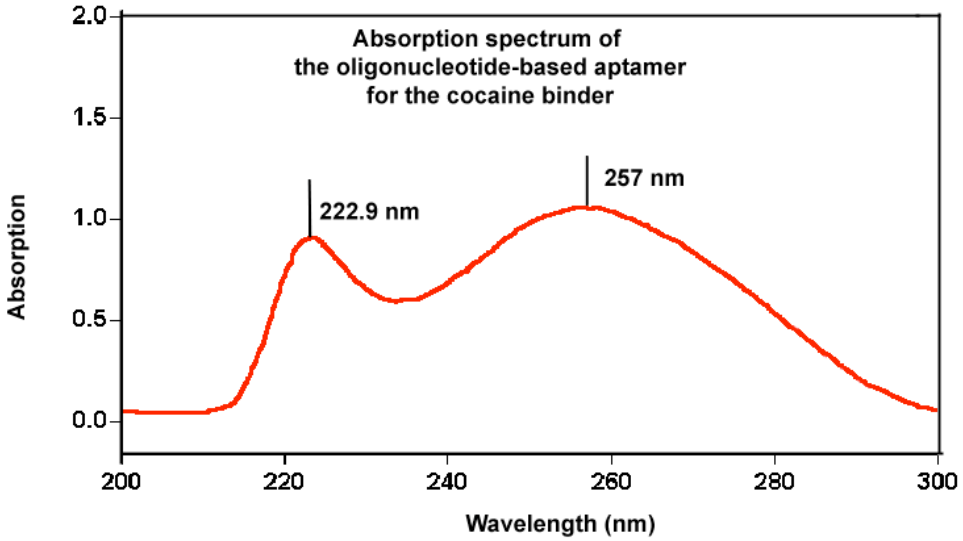

Figure 5.1: UV-Vis spectrum of aptamer in triethylammonium acetate (TEAA) buffer with peak near 260 nm. The 223 nm peak is the TEAA buffer spectrum.

formation of SAMs. At the temperature higher than 25^o C the rate of non-specific binding desorption and the thiols adsorption increases. The most often used solvent in SAMs formation is ethanol. It has been reported that the structure of water, which is common solvent in biological molecules, may prevent the molecules from adsorption on the surface. Since the concentration of the aptamer, which is dissolved in water-based TEAA buffer, is approximately 10 times less than the concentration mentioned above and that the immersion is placed in -4^o C, the coating time needs to be increased to obtain similar dense coverage. Three-day immersion is found to be sufficient. It gives a decrease in the QCM frequency of 40 Hz on average which corresponds to 160 ng of aptamer. Given the aptamer molecular weight of 12,273.6 gr/mol and the dimension of the gold electrode of the QCM, the obtained density of the aptamer is 1.1×10^{13} molecules/cm^2. This number is less dense than that published Love *et. al.* that suggets a typical surface density of approximately 4.5×10^{14} molecules/cm^2 for self assembly monolayers created from alkanethiols on gold. The less dense of the aptamer on the gold surface can be explained due to the larger size of the its molecules compared to pure alkane chain molecules. The steric bulk of the larger biomolecules attached to the thiol prevents the formation of an organized self assembly monolayer. Instead, a disordered and less dense layer is developed. Fig. 5.2 shows the difference in the organization and packing density of SAMs for different size of terminal groups [66].

5.2 Relative cocaine concentration measurement using quartz crystal microbalance

The experiment was started with a new, clean QCM which was immersed in the aptamer for five days resulting a change in frequency of 43 Hz. As a control, the QCM was submerged in distilled water for 30 minutes, dried under N_2 stream, followed by reading its resonant frequency. This process was repeated for several times. Small changes of frequency also appeared for the first QCM submersion in distilled water, in which the frequency increases in the first water immersion implying that there was a decrease in mass. This can be

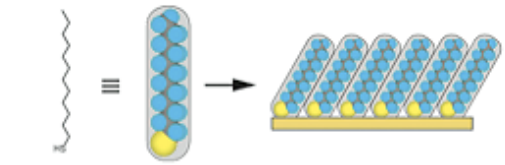

(a)

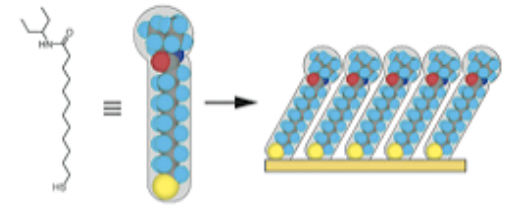

(b)

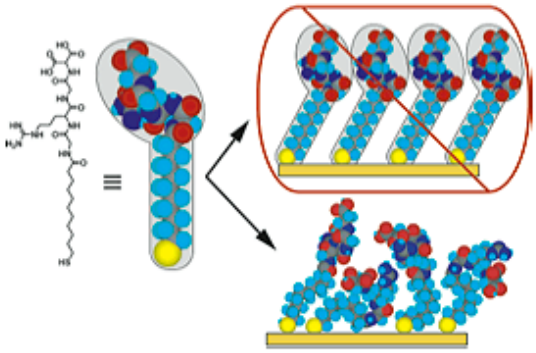

(c)

Figure 5.2: Packing density and organization of SAMs of different sizes terminal groups attached to the alkanethiols [66]. (a) Small size groups such as $-CH_3$ and –CN form fully ordered SAMs. (b) Medium size groups as the branched amide shown above creates slightly disordered SAMs. (c) Larger size groups as for biomolecules (proteins, antibodies, etc.) produce disordered and less dense SAMs.

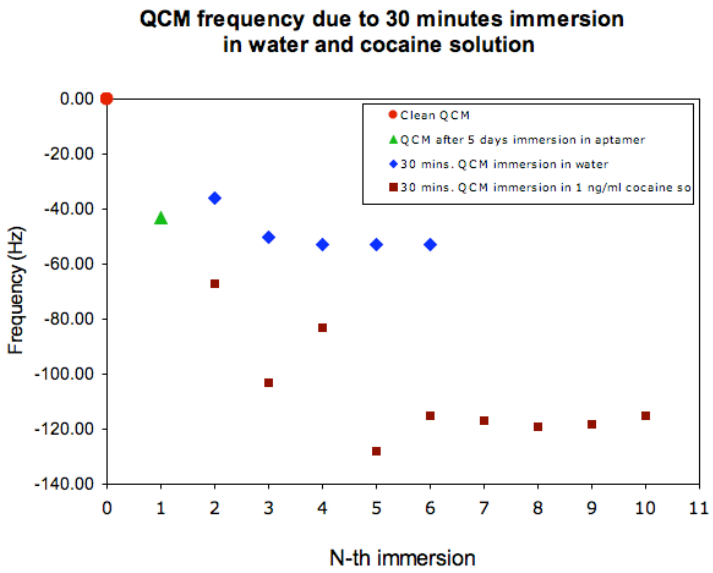

Figure 5.3: Change in resonant frequency of QCM due to immersion in 0.001μ g/ml cocaine solution.

caused by elimination of any contaminant and/or debris on the crystal surface which was not thoroughly rinsed upon removing it from the aptamer solution.

Afterwards, a similar procedure was carried out for the same QCM in 0.001 μg/ml cocaine solution. Changes in resonant frequency were observed as shown Fig. 5.3. After the fifth immersion, frequency changes were very small and that they were negligible, i.e. less than 5 Hz frequency change in comparison to the QCM resonant frequency, which is 6 MHz. The small frequency changes imply the saturation of the aptamer binding sites. The total change of frequency measured from the last crystal immersion in the water to the last immersion in the cocaine is about 62 Hz which corresponds to 248 ng of cocaine bind onto the QCM gold surface.

The same experiment was done for a different, clean, new QCM. Six days of immersion of the second QCM in the aptamer gives a frequency change of 46 Hz. Consecutive thirty minutes of dipping, rinsing, and drying method using 0.05 μg/ml cocaine solution produced

a total change in resonant frequency of 70 Hz. This experiment has proven the high affinity of the aptamer to cocaine.

5.3 In vitro relative cocaine concentration measurement in a flow controlled system using the wired sensor

Relative cocaine concentration measurement

First, both syringes were filled with water. Setting the six port valve in the load mode, distilled water from syringe B was flown to the channel until a stable signal with minimum drift was reached. The pump rate was set to 50 μl/min. Once the signal was stabilized, the 1-ml loop was filled with water from syringe A, the mode was switched to inject mode. In this mode, a continous solution flowed to the sensor in which the water from syringe B would push the water in the 1-ml loop from syringe A. As illustrated in Fig. 5.4, which plots the surface stress of each microcantilever over time, the 20 minutes line that marks the end of 1-ml loop, no change in signal is observed as expected. Later, distilled water in syringe B was replaced with cocaine solution starting at a very low concentration i.e. 0.001 μg/ml or 1 ng/ml. The experiment was carried out three times for each concentration. Since output data from bridge A does not vary much from that of bridge B, data from both bridges (total of six data sets) were averaged to determine the surface stress values.

Unless stated otherwise, the parameters used for data acquisition were the following update rate 8.33 Hz, polarity bipolar, gain 128, and reference of 2.50 V. The output signal is read in voltage. A conversion from voltage to surface stress is performed using the equations Eq. 3.5 and Eq. 2.14. The signal also suffered from thermal drift which was then eliminated by removing its background. Fig. 5.4 shows the surface stress over time for cocaine concentration of 0.001, 0.01, and 0.1 μg/ml for the same device. For approximately 10 minutes after introducing the cocaine solution, the sensor experienced positive surface stress followed by a decreasing surface stress. This can be explained as follows: at the small amount of cocaine bound to the microcantilever, the molecules tend to attract each other

Table 5.1: Average change in surface stress for different cocaine concentration for detection using wired sensor in a flow controlled system.

Cocaine concentration μg/ml	$\Delta\sigma_s$ mN/m
0.001	0.12 ± 0.04
0.0025	-0.17 ± 0.07
0.005	-0.26 ± 0.08
0.01	-0.38 ± 0.11
0.025	-0.51 ± 0.07
0.05	-0.54 ± 0.15
0.1	-0.72 ± 0.12
0.25	-0.99 ± 0.29
0.5	-1.07 ± 0.11

causing the cantilever to bend towards its surface, hence the positive surface stress. As the number of cocaine molecules increases, they tend to repel each other due to the dipole moment. As a result, the cantilever bends aways from its surface causing the surface stress to decrease.

Table 5.1 and Fig. 5.5 summarize the means and standard deviations of the shift in surface stress of each microcantilever over the same period of time as in Fig. 5.4, i.e. 100 minutes, for different cocaine concentration. Limit of detection of 1 μg/ml or 1 ng/ml proves the sensitivity of the sensor to detect cocaine. This number is comparable to detection performed using gas/liquid chromatography, and mass spectrophotometry. In addition, it shows that there is a rapid change in the surface stress at lower cocaine concentration. Saturation signal occurring at higher concentration is attributed to depletion of the binding sites of the aptamer.

The above experiment was repeated one month later. However, inconsistent results were obtained for each concentration. The aptamer may not be as efficient in binding with cocaine molecules as when it was freshly prepared.

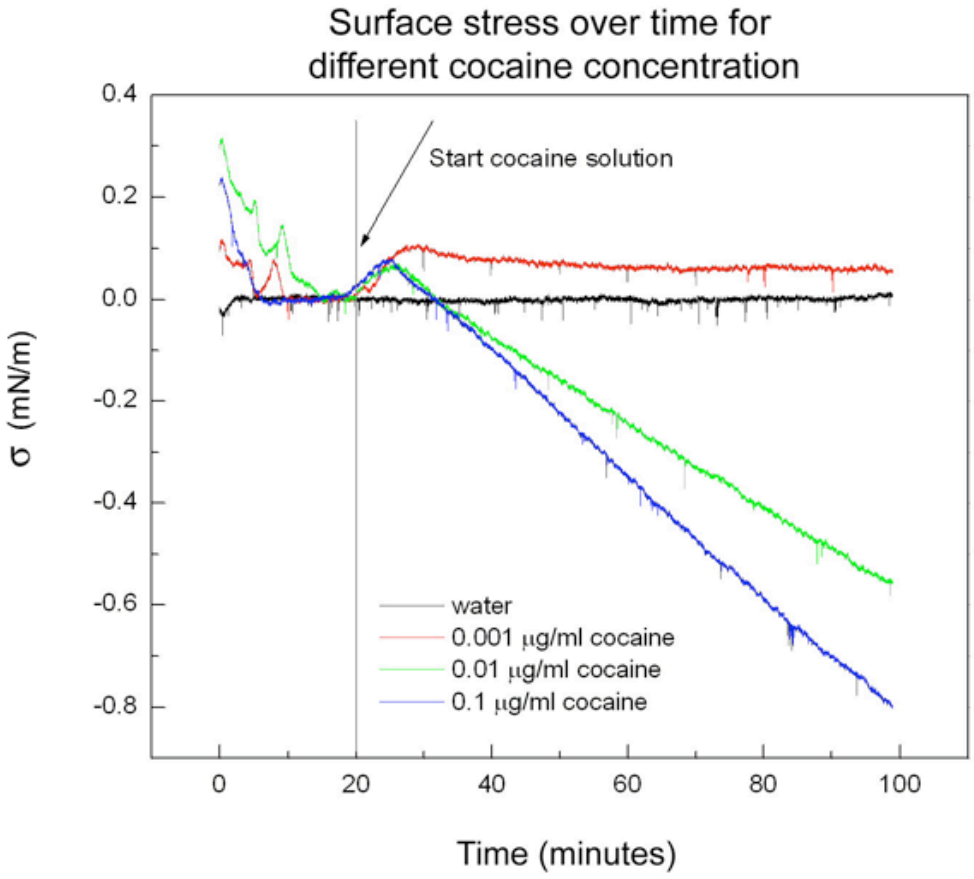

Figure 5.4: Result data of cocaine detection for wired sensor in a flow controlled system for three different cocaine concentration.

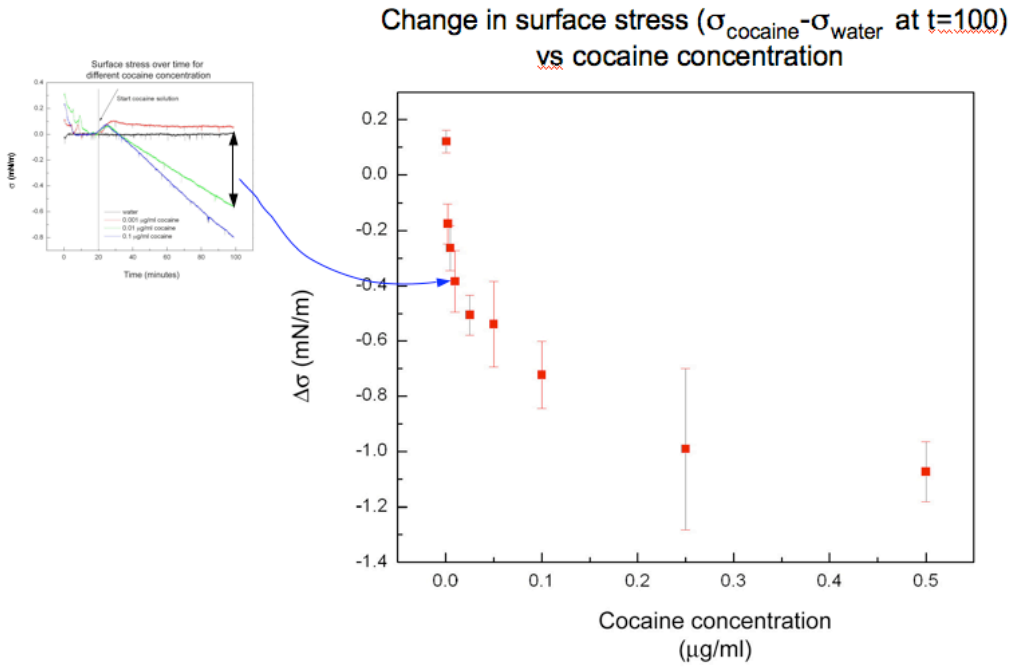

Figure 5.5: Average change in surface stress for different cocaine concentration for detection using wired sensor in a flow controlled system.

Non-cocaine binding test

Alcohol was used as the non-cocaine binding to the aptamer. It is common for cocaine users to also drink alcohol while consuming the drug. Different alcohol concentrations were tested for this experiment based on the standard blood alcohol content (BAC) [92] which is measured as mass of alcohol per volume. For example, a BAC of 0.02 percent, in which a subtle effect can be detected through special tests, means 0.02 grams of alcohol per 210 liter of breath, or 0.02 grams of alcohol per 100 ml of blood. Fig. 5.6 displays the response of the sensor using alcohol at BAC level of 0.02, 0.04, 0.08*, and 0.16 percent. As in the cocaine experiment, the alcohol was introduced to the sensor at time $t = 20$ minutes following the distilled water flow. No alcohol is detected at BAC level of 0.02 to 0.08 percent, however, signal change is observed at 0.16 percent. It is not known for sure the deflection is due to alcohol attachment to the aptamer or due to change in temperature with the presence of the alcohol at the higher level.

The rest of this chapter will cover wireless sensor whose output signals are displayed in decimal representation of the binary code from the receiver. Conversion from the binary codes to the Wheatstone bridge voltage outputs, to changes in resistance and to surface stress of the microcantilevers involve many parameters and variables. Therefore, data reading and analysis will be done based on this numbers.

5.4 In vitro relative cocaine concentration measurement in a flow controlled system using the wireless sensor

As mentioned in Chapter 4, similar procedure used for the in vitro detection in a flow controlled system using the wired sensor was used here. Beside the difference in the electronic read-out components, the signal output is read every 8 seconds for the wireles sensor. Other parameters for data acquisition and pump rate are maintained the same. The water-water

*BAC level of 0.08 percent is the lowest limit for driving under influence (DUI) in the 50 states in the United States.

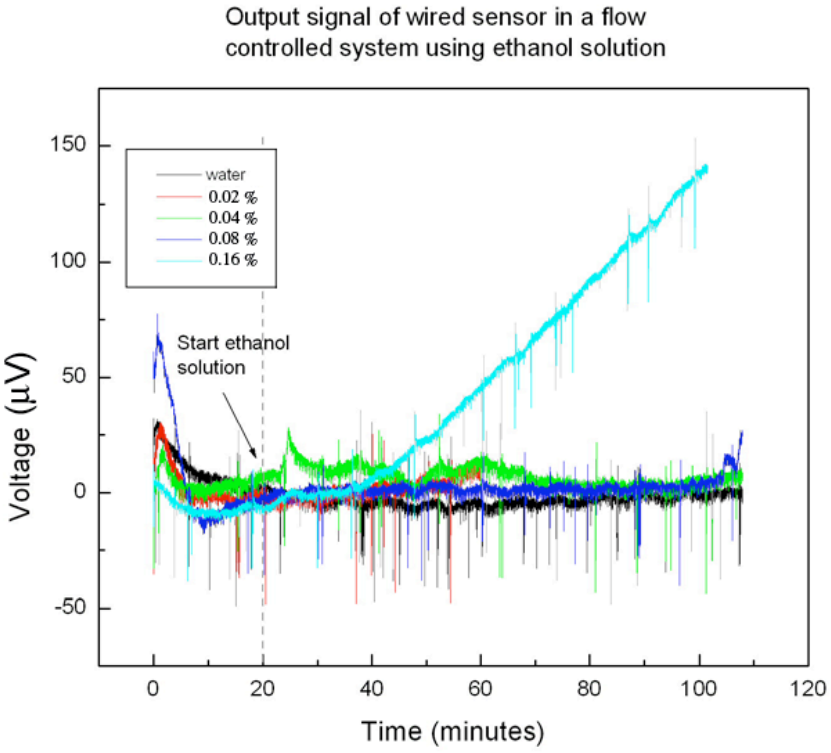

Figure 5.6: Signal output for alcohol detection using wired sensor in a flow controlled system.

experiment was omitted as it can be seen from previous experiment using the wired sensor that the aptamer does not response to the water. The change in sensor signal is determined by subtracting the water-only output from the output with the presence of cocaine at time t equals to 1 hour 40 minutes. Fig. 5.7 shows the output data of the sensor for cocaine concentration of 0.01, 0.1, and 0.5 μg/ml.

Comparing the output signals from both the wired and wireless sensor in a flow controlled system, we find that one is the vertical mirror of the other. The output in the wireless signal displays negative slope follows by increase in the signal value as oppose to the signal output in the wired signal as illustrated in Fig. 5.4. This can be explained by the difference in the wiring from the modified Wheatstone bridge outputs to the analog input pins of the analog to digital converter chip between the both sensors. For example, as described in Fig. 5.8, the left output voltage of the bridge is connected to the AIN(+) in one sensor but to the AIN(-) in the other sensor. This connection is done arbitrary and it only causes the polarity to differ; however, it does not change the direction of the cantilever bending. As in section 5.3, it is also shown here the means and standard deviations of cantilever deflection at t = 1 hour 40 minutes minus that before t = 20 minutes, i.e. before cocaine solution is introduced to the sensor for all concentration tested in this experiment (see Table 5.2 and Fig. 5.9). The sensor experienced approximately the same amount of change in output signal due to cocaine at the concentrations between 0.0025 to 0.01 μg/ml, but quite rapid changes observes at higher concentration.

5.5 In vitro relative cocaine concentration measurement in a stagnant solution using the wireless sensor

Due to the considerably low vapor pressure of cocaine, the capsule manufactured by Flextronics requires to be immersed in liquid. The experiment was started by filling the petri dish with 70 ml distilled water. This amout of water is enough to submerge the entire capsule. A certain amount of cocaine solution was gradually introduced to produce the

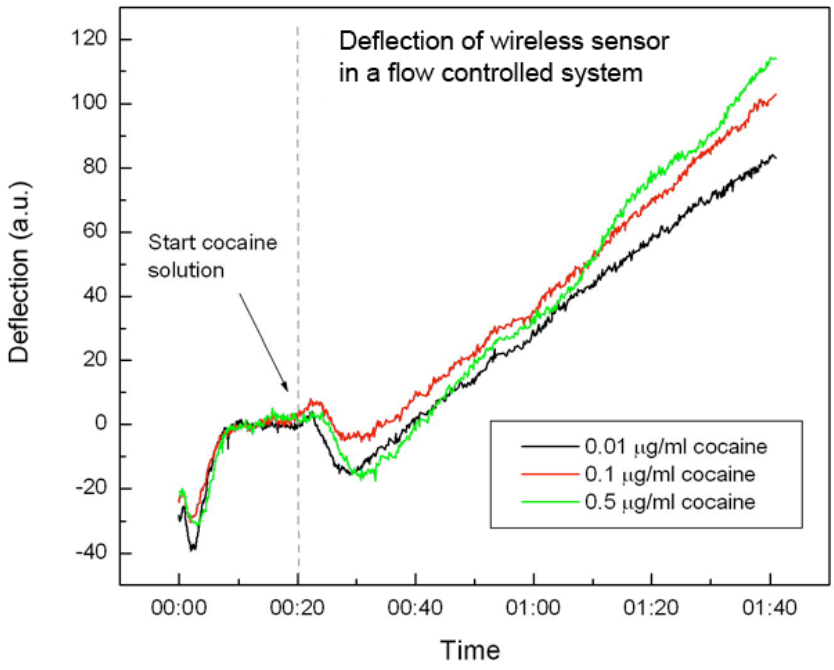

Figure 5.7: Result data of cocaine detection for wireless sensor in a flow controlled system for three different cocaine concentration.

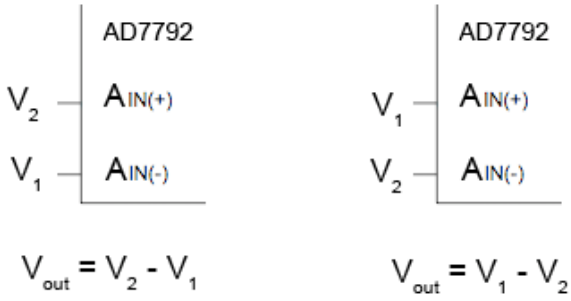

Figure 5.8: Arbitrary connection from the Wheatstone bridge voltage out to AD7792/3 AIN pins results in different voltage polarity.

Table 5.2: Average change in output signal for different cocaine concentration for detection using wireless sensor in a flow controlled system.

Cocaine concentration μg/ml	$\Delta\sigma_s$ a.u.
0.001	71.33 ± 2.31
0.0025	95 ± 7.07
0.005	92.2 ± 2.69
0.01	92.5 ± 8.66
0.025	98.44 ± 7.84
0.05	103.07 ± 5.61
0.1	114.49 ± 0.72
0.25	133 ± 8.12
0.5	146.67 ± 6.11

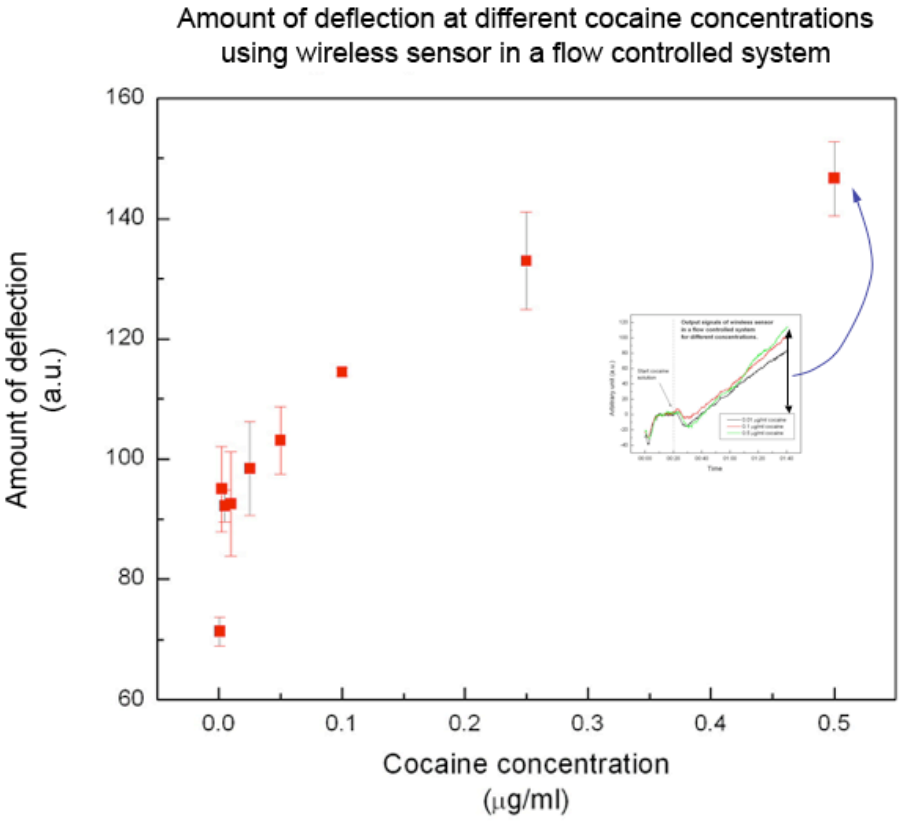

Figure 5.9: Mean plot of change in output signal for different cocaine concentration for detection using wireless sensor in a flow controlled system.

same various cocaine concentration as used in previous experiments. Unfortunately, a very noisy signal was observed in this experimental setup which could possibly due to distilled water entering the electronic compartment either through dispersion on the sensor board or around the capsule casing. To overcome this problem, a sheet of parafilm was placed between the upper and lower sensor board. The sheet needs to be larger than area of the capsule such that when the top and bottom casing are fastened together, there is extra sheet showing around the capsule. A heat shrink tubing with a cutout created around the capsule window, where the microcantilevers are exposed, was used to enclosed the capsule. The capsule was then heated at the maximum temperature of 30^oC to prevent damaging the microcantilevers and shortened the lifetime of the aptamer . The purpose for the parafilm sheet is to give extra sealant around the casing after being heated. The problem, nevertheless, still present despite the effort to provide good sealant to the sensor.

It was discovered that the fluctuating signal is attributed to the silver conductive epoxy that is used to glue down the microcantilevers to the gold bond pads on the printed circuit board. This epoxy expands or swells up when it is exposed to humidity, causing the electrical connection of the arrays to slowly break away from the printed circuit board. In addition, the resistance of the microcantilever gradually becomes larger toward infinity, in which the read-out values of the resistance are no longer correct. To resolve this problem, the original microcantilevers mounted on the sensor board were replaced by microcantilevers mounted on individual printed circuit board made by Cantion, Inc. Thus, similar wireless sensor used in the flow controlled system was utilized in this experiment except there is no flow channel built over the microcantilever arrays. Since the new form of the device causes the sensor unable to fit into the capsule casing, to isolate the electronic from the distilled water, the sensor was secured on the petri dish as illustrated in Fig. 5.10.

This new experimental setup resulted in more stable signal. The experiment was started by filling the petri dish with 70 ml distilled water. Cocaine solution was then introduced to the sensor after the signal was stabilized. Fig. 5.11 represents the change in the signal for cocaine concentrations of 0.001, 0.02, 0.1 and 1.0 μg/ml. The plots show that the sensor

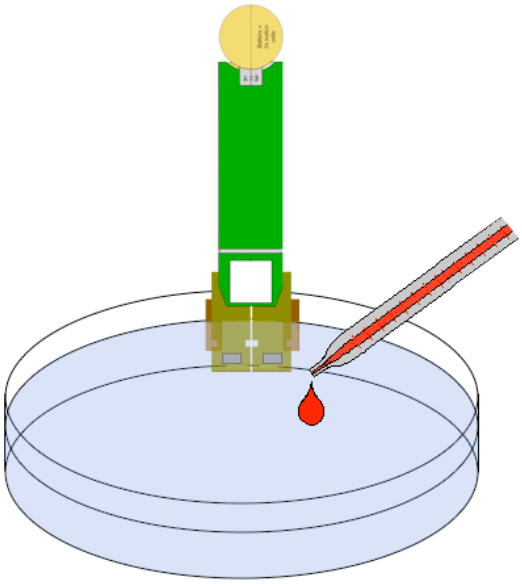

Figure 5.10: Experimental setup of in vitro cocaine detection in a stagnant solution.

was still able to detect cocaine at the low concentration via diffusion. Surprisingly, the plots show that as the cocaine concentration is increased, the cantilever deflection becomes smaller. This may be explained that the cocaine molecules are more difficult to detach from the aptamer when the sensor is placed in a stagnant solution than when it is placed is in a flow controlled system. More future work can be conducted to understand this phenomenon.

5.6 In vivo cocaine detection in Wistar rats

In this experiment, cocaine injected to the Wistar rats was detected. However, the absolute concentration of the cocaine was not able to be measured. The main concern in this experiment was to have the interstitial fluid enter the microcantilever arrays without having the fluid reach the electronic components. Therefore, a new embodiment of the sensor was done. The electronics are sealed off from the liquid water and then only the cantilevers are exposed to liquid. However, as mentioned in previous experiment, the cantilever arrays are attached to the printed circuit board by an epoxy that is not 100 percent water resistant. In order to circumvent this problem, mounted cantilever arrays made by Cantion, Inc. were soldered to the printed circuit board. The printed circuit board no longer fit in the original yellow capsule due to the nature of the new electrical connections. The modified capsule was placed in a plastic centrifuge tube that was not sealed from liquid water. The end of the centrifuge tube was plugged with a mesh to minimize animal tissue from entering the sensor chamber. To protect the electronics from the liquid, the capsule (excluding the cantilever arrays) was coated with an epoxy (fiberglass resin). The battery was not epoxied since it would drain before the capsule would be implanted. Two wires were connected to the battery terminals so that an external battery could be used in data acquisition for cocaine detection in Wistar rats. The modified capsule, shown in Fig. 5.12, was implanted in Wistar rats from Dr. William McBride's group at the Institute of Psychiatric Research, Indiana University-Purdue University Indianapolis.

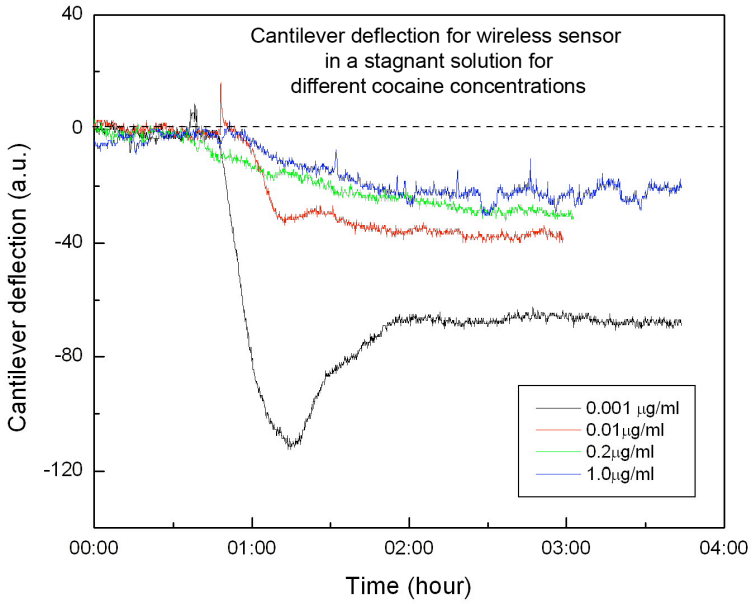

Figure 5.11: Cantilever deflection of wireless sensor in a stagnant solution for various cocaine concentrations.

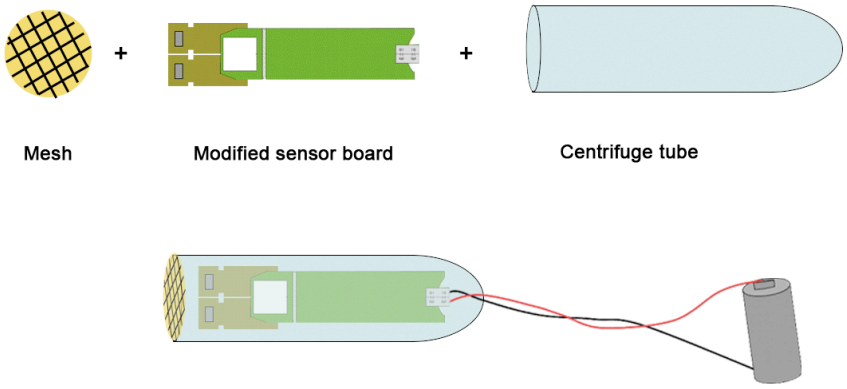

Figure 5.12: The modification result of the implanted sensor in male Wistar rats. The battery is connected externally, however, data transmission is still wireless.

A male Wistar rat was implanted with capsule 59 (external battery/modified capsule) on December 6, 2007 at 9:40 AM. The rat was given a lengthened surgical recovery time to also allow for sensor stabilization. The rat was intraperitoneally injected with a 10 ml/kg dose of 20 mg/ml cocaine hydrochloride solution in water at 11:59 AM. The rat had a mass of 403 g. As shown in Fig. 5.13, there was a good response from the sensor that can be seen with the change in slope in the data. The rat was given a second dose of 20 ml/kg cocaine hydrochloride solution at 2:54 PM. There was no response from the sensor for the second dose. This lack of response may be attributed to the depletion of available binding sites for cocaine. Generally there should still be available binding sites for multiple cocaine injections, but this can vary with the coating process. Also, the use of the epoxy could have heated the capsule above the optimum temperature for maintaining a long aptamer lifetime. The cocaine detection can be greatly improved with better epoxy application and with a better container for the printed circuit board and electronics. The interstitial fluid did not uniformly cover the cantilevers especially with the centrifuge tube capsule.

Another Wistar rat with mass of 422 g was implanted with capsule 612 on December 7, 2007 at 8:47 AM. This rat was also given a lengthened surgical recovery time to also allow for sensor stabilization. The rat was intraperitoneally injected with a 10 ml/kg dose of 20 mg/ml cocaine hydrochloride solution in water at 12:10 PM. There was no response with the first dose. A second dose of 20 ml/kg was given at 3:55 PM where there was a large change in signal (Fig. 5.14 and Fig. 5.15).

From the three plots, the sensors response are relatively quickly which agree to the information provided by the Drugs and Human Performance Fact Sheets [93]. It states that intravenous administration of single 32 mg doses of cocaine produced an average peak blood concentration of 0.31 μg/ml of cocaine within 5 minutes.

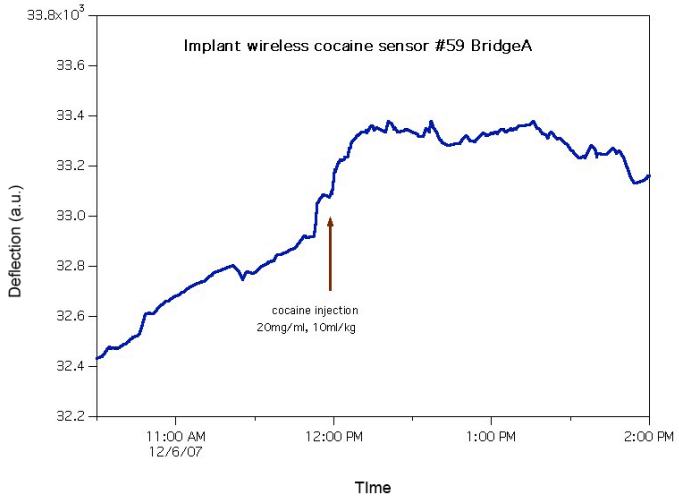

Figure 5.13: Signal deflection of sensor 59 bridge A implanted in a Wistar rat.

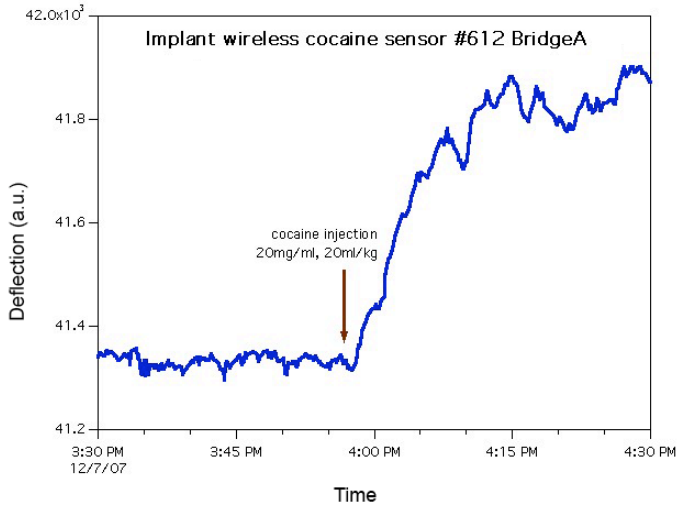

Figure 5.14: Signal deflection of sensor 612 bridge A implanted in a Wistar rat.

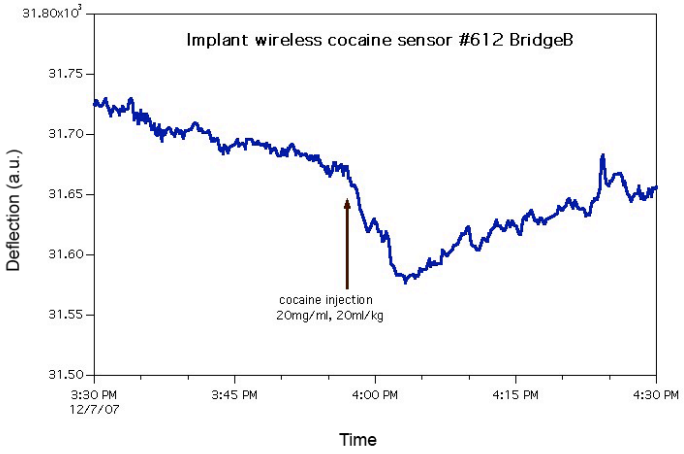

Figure 5.15: Signal deflection of sensor 612 bridge B implanted in a Wistar rat.

Chapter 6

Summary and Future Work

Measurement of cocaine concentration in the human body has been the focus of research to improve the understanding of the drug use. Current means of measurement are done by taking the blood and urine samples and performing analytical chemistry. This method is very expensive, time consuming, labor intensive, and there is possibility of mismatch between a subject and his or her sample. Therefore, a new approach for in detecting and measuring cocaine which, automatically reports the presence of cocaine, is important.

This objective has been achieved by designing a cocaine biosensor which is low cost, fast, simple, and small, enabling the device the sensor to be implanted in the body. The sensor uses piezoresistive microcantilever arrays as its transducer and oligonucleotide-based aptamer coated on the cantilever as the cocaine receptor. Off-the-shelf electronic components are chosen for simplicity, which including an AD7792/3 analog to digital converter, MSP430F1232 microprocessor, and TH72011 transmitter chip. Data transmission is done via telemetry, removing the need of using any discomforting wire.

Dissertation has developed and tested step by step the process towards shaping the final implantable device. The contributions of this dissertation include:

- optimizing the coating process of the cocaine receptor using the quartz crystal microbalance (QCM),

- evaluating cocaine binding to the aptamer using the QCM,
- in vitro testing of the sensor prototype to determine the sensitivity and specifity of the sensor,
- measuring relative cocaine concentration – also in vitro,
- verifying the electronic read-out of the capsule, especially its wireless data transmission, and
- implanting the sensor into cocaine-administered Wistar rats.

Three days immersion time in the aptamer solution give an optimum molecule density. This number is then used as the minimum time for coating the microcantilevers. The aptamer has been proven to bind to the cocaine after being immobilized on the gold surface. The wired sensor, which is the prototype of the capsule, is used to determine the limit of detection of the cocaine in the solution. Cantilever bending at cocaine concentration of 1 μg/ml or 1 ng/ml is shown, which are comparable number concentrations as those detected by other methods. This proves the sensitivity of the microcantilevers in detecting the drug in the solution. In addition, the relative concentration of the cocaine concentration can be measured using this prototype with a resolution of 1 ng/ml.

The experiment using the wireless sensor, both in vitro and in the Wistar rats, shows that data transmission via telemetry works very well. The sensor, however, had to be modified due to a problem with the electrical epoxy that attaches the microcantilever arrays to the capsule board. The experiments that were conducted in a flow controlled system and in a stagnant solution exhibit the same limit of detection of the cocaine concentration. For the in vivo experiment, a fast response is observed upon injecting the cocaine to the Wistar rats. However, there were some occasions when the sensors did not respond after injection. This could be attributed to depletion of the binding sites, or to thermal damage leading to shortened aptamer lifetime and occuring during the processing of the fiberglass resin covering the capsule board.

These observations allow us to indicate the areas where changes will yield an improved sensor. For example:

- utilizing the right conductive epoxy which does not swell up when exposed to humidity to attach the microcantilever array chips to the capsule board,
- alternatively, wired-bonding the microcantilevers to the capsule board, and
- fabricating new capsule or container that isolating the electronics from any fluid.

Furthermore, the capsule can be made smaller by selecting a chip that contains microprocessor, analog to digital converter, and transmitter in a single device, such as CC1010 chip from Texas Instruments.

Bibliography

Bibliography

[1] P. Fernández, C. Vázquez, L. Morales, and A.M. Bermejo. Analysis of opiates, cocaine and metabolites in urine by high-pereformance liquid chromatography with diode array detection (HPLD-DAD). *Journal of Applied Toxicology.*, 25:200–204, 2005.

[2] Karl B. Scheidweiler, Edward J. Cone, Eric T. Moolchan, and Marilyn. Huestis. Dose-related distribution of codeine, cocaine, and metabolites into human hair following controlled oral codeine and subcutaneous cocaine administration. *The Journal of Pharmacology and Experimental Therapeutics.*, 313:909–915, 2005.

[3] P. Fernández, M. Leòn, A.M. Bouzas, A.M. Bermejo, and M. J. Tabernero. Use of high-performance liquid chromatography for the determination of cocaine and benzoylecgonine in human hair. *Journal of Liquid Chromathography and Related Technologies.*, 26(12):2003–2012, 2003.

[4] Sherri L. Kacinko, Allan J. Barnes, Eugene W. Schwilke, Edward J. Cone, Eric T. Moolchan, and Marilyn. Huestis. Disposition of cocaine and its metabolites in human sweat after controlled cocaine administration. *Clinical Chemistry*, 51(11):2085–2094, 2005.

[5] M. Yonamine, N. Tawil, R. L. de Moraes Moreau, and O. A. Silva. Solid-phase microextraction-gas chromatography-mass spectrometry and headspace-gas chromatography of tetrahydrocannabinol, amphetamine, methamphetamine, cocaine, and ethanol in saliva samples. *Journal of Chromatrography B*, 789:73–78, 2003.

[6] Lei. Sun, Gene. Hall, and Chyan E. Lau. Solid-phase micro-extraction-gas chromatography-mass spectrometry and headspace-gas chromatography of tetrahydrocannabinol, amphetamine, methamphetamine, cocaine, and ethanol in saliva samples. *Journal of Chromatrography B*, 745:315–323, 2000.

[7] K. Watanabe, K. Okada, H. Oda, K. Furuno, Y. Gomita, and T. Katsu. New cocaine-selective membrane electrode. *Analytica Chimica Acta*, 316:371–375, 1995.

[8] L. Campanella, C. Colapicchioni, M. Tomassetti, A. Bianco, and S. Dezzi. A news ISFET device for cocaine analysis. *Sensors and Actuators. B, Chemical*, 24–25:188–193, 1995.

[9] L. Campanella, C. Colapicchioni, M. Tomassetti, and S. Dezzi. Comparison of three analytical methods for cocaine analysis of illicit powders. *Journal of Pharmacheutical and Biomedical Analysis*, 14:1047–1054, 1996.

[10] Yanbin. Li. Biosensors. In CIGR The International Commission of Agricultural Engineering., editor, *CIGGR Handbook of Agricultural Engineering Vol. VI Information Technology.*, pages 52–93. 2006.

[11] C. G. Bauer, A. V. Eremenko, A. Kühn, K. Kürzinger, A. Makower, and F. W. Scheller. Automated amplified flow immunoassay for cocaine. *Analytical Chemistry*, 70:4624–4630, 1998.

[12] A. A. Suleiman and Y. Xu. An amperometric immunosensor for cocaine. *Electroanalysis*, 10:240–243, 1998.

[13] S.D. Jayasena. Aptamers: An emerging class of molecules that rival antibodies in diagnostics. *Clinical Chemistry*, 45:1628–1650, 1999.

[14] Brian R. Baker, Rebecca Y. Lai, McCall S. Wood, Elaine H. Doctor, Alan J. Heeger, and Kevin W. Plaxco. An electronic, aptamer-based small-molecule sensor for the

rapid, label-free detection of cocaine in adulterated samples and biological fluids. *Journal of the American Chemical Society*, 128(10):3138–3139, 2006.

[15] P. J. Devine, N. A. Anis, J. Wright, S. Kim, A. T. Eldefrawi, and M. E. Eldefrawi. A fiber-optic cocaine biosensor. *Analytical Biochemistry*, 227:216–224, 1995.

[16] M. N. Stojanovic, P. de Prada, and D. W. Landry. Aptamer-based folding fluroscent sensor for cocaine. *Journal of the American Chemical Society*, 123:4928–4931, 2001.

[17] M. N. Stojanovic and D. W. Landry. Aptamer-based colorimetric probe for cocaine. *Journal of the American Chemical Society*, 124:9678–9679, 2002.

[18] J. Liu and Y. Lu. Fast colorimetric sensing of adenosine and cocaine based on a general sensor design involving aptamers and nanoparticles. *Angewandte Chemie*, 117:1–5, 2005.

[19] B. S. Attili and A. A. Suleiman. A piezoelectric immunosensor for the detection of cocaine. *Microchemical Journal*, 54:174–179, 1996.

[20] J. Halámek, A. Makower, P. Skládal, and F. W. Scheller. Highly sensitive detection of cocaine using a piezoelectric immunosensor. *Biosensor and Bioelectronics*, 17:1045–1050, 2002.

[21] J. Halámek, A. Makower, K. Knösche, P. Skládal, and F. W. Scheller. Piezoelectric affinity sensors for cocaine and cholinesterase inhibitors. *Talanta*, 17:337–342, 2005.

[22] T. Frisk, D. Rönnholm, W. van der Wijngaart, and G. Stemme. Fast narcotics and explosives detection using a microfluidic sample interface. In *The 13th International Conference on Solid-State Sensors, Actuators and Microsystems*, pages 2151–2154, Seoul, Korea, June 2005.

[23] D.D. Stubbs, S. Lee, and W.D. Hunt. Investigation of cocaine plumes using surface acoustic wave immunoassay sensors. *Analytical Chemistry*, 75:6231–6235, 2003.

[24] D.D. Stubbs, S. Lee, and W.D. Hunt. Vapor phase detection of a narcotic using surface wave acoustic wave immunoassay. *IEEE Sensors Journal*, 5(3):335–339, 2005.

[25] N. Nath, M. Eldefrawi, J. Wright, D. Darwin, and M. Huestis. A rapid reusable fiber optic biosensor for detecting cocaine metabolites in urine. *Journal of Analytical Toxicology*, 23:460–467, 1999.

[26] T. Thundat, P. I. Oden, and R. J. Warmack. Microcantilever sensors. *Microscale Thermophysical Engineering*, 1:185–199, 1997.

[27] G. Binnig, C. F. Quate, and Ch. Gerber. Atomic force microscopy. *Physical Review Letters*, 56(9):930–933, 1986.

[28] J. Koeser, P. Shahgaldian, M. Bammerlin, F. M. Battiston, and U. Pieles. Time resolved analysis of molecular interactions using nanomechanial cantilever sensors. In *Journal of Physics: Conference Series*, 61, pages 612–617. International Conference on Nanoscience and Technology (ICN&T 2006), 2007.

[29] P. A. Rasmussen. *Cantilever-based sensors for surface stress measurements.* PhD thesis, Department of Micro and Nanotechnology, Tehnical University of Denmark, Lyngby, Denmark, August 2003.

[30] T. Thundat, E. A. Wachter, S. L. Sharp, and R. J. Warmack. Detection of mercury vapor using resonating cantilevers. *Applied Physics Letter*, 66:1695–1697, 1995.

[31] D. Lange, A. Koll, O. Brand, and H. Baltes. Cmos chemical microsensors based on resonant cantilever beams. In *Proceeding of the SPIE – The Internationl Symposium for Optical Engineering*, volume 3328, pages 233–243, 1998.

[32] A. Hierlemann, D. Lange, C. Hagleitner, N. Kernes, A. Koll, O. Brand, and H. Baltes. Application-specific sensor systems based on cmos chemical microsensors. *Sensors and Actuators B: Chemical*, 70(1–3):2–11, 2000.

[33] B. H. Kim, F. E. Prins, D. P. Kern, S. Raible, and U. Weimar. Multicomponent analysis and prediction with a cantilever array based gas sensor. *Sensors and Actuators. B, Chemical*, 78(1–3):12–18, 2001.

[34] J. D. Adams, G. Parrott, C. Bauer, T. Sant, L. Manning, M. Jones, M. Rogers, D. McCorkle, and T. L. Ferrell. Nanowatt chemical vapor detection with a self-sensing, piezoelectric microcantilever array. *Applied Physics Letters*, 83:3428–3430, 2003.

[35] J. K. Gimzewski, Ch. Gerber, E. Meyer, and R. R. Schlittler. Observation of a chemical reaction using a micromechanical sensor. *Chemical Physics Letters*, 217(5–6):589–594, 1994.

[36] J. Barnes, R. J. Stephenson, M. E. Welland, C. Gerber, and J. K. Gimzewski. Photothermal spectroscopy with femtojoule sensitivity using a micromechanical device. *Nature*, 372:79–81, 1994.

[37] R. Berger, E. Delamarche, H. P. Lang, J. K. Gimzewski, E. Meyer, and H.-P. Güntherodt. Surface stress in the self-assembly of alkanethiols on gold. *Science*, 276:2021–2024, 1997.

[38] H. Jensenius, J. Thaysen, A. A. Rasmussen, L. H. Veje, O. Hansen, and A. Boisen. A microcantilever-based alcohol vapor sensor-application and response model. *Applied Physics Letters*, 76(18):2615–2617, 2000.

[39] J. Thaysen, R. Marie, and A. Boisen. Cantilever-based biochemical sensor integrated in a microliquid handling system. In *Micro Electro Mechanical Systems 2001. The* 14^{th} *IEEE International Conference*, pages 401–404, 2001.

[40] C. P. Cheney, A. Wig, D. L. Hedden, A. Gehl, A. L. Lereu, R. H. Farahi, S. R. Hunter, and T. L. Ferrell. Ethanol vapor detection in saline solution using piezoresistive microcantilevers. *Review of Scientific Instruments*, 77(9):095101–095105, 2006.

[41] G. Binnig, H. Rohrer, Ch. Gerber, and E. Weibel. Surface studies by scanning tunneling microscopy. *Physical Review Letters*, 49:57–61, 1982.

[42] T. Göddenhenrich, H. Lemke, U. Hartmann, and C. Heiden. Force microscope with capacitive displacement detection. *Journal of Vacuum Science and Technology A*, 8:383–387, 1990.

[43] Y. Martin, C. C. Williams, and H. K. Wickramasinghe. Atomic force microscope-force mapping and profiling on a sub 100-$\ddot{A}$ scale. *Journal of Applied Physics*, 61:4723–4729, 1987.

[44] D. Royer, E. Dieulesaint, and Y. Martin. Improved version of a polarized beam heterodyne interferometer. *Proceedings of IEEE Ultrasonics Symposium*, pages 432–435, 1985.

[45] C. Schönenberger and S. F. Alvarado. A differential interferometer for force microscopy. *Review of Scientific Instruments*, 60(10):3131–3134, 1989.

[46] D. Sarid, D. Iams, V. Weissenberger, and S. Bell. Compact scanning-force microscope using a laser diode. *Optics Letters*, 13(12):1057–1059, 1988.

[47] G. Meyer and N. M. Amer. Novel optical approach to atomic force microscopy. *Applied Physics Letter*, 53:1045–1047, 1988.

[48] N. Tortonese, R. C. Barrett, and C. F. Quate. Atomic resolution with an atomic force microscope using piezoresistive detection. *Applied Physics Letter*, 62(8):834–836, 1993.

[49] G. G. Stoney. The tension of metallic films deposited by electrolysis. *Proceedings of the Royal Society of London. Series A*, 82(553):172–175, 1909.

[50] J. Thaysen. *Cantilever for bio-chemical sensing integrated in a microliquid handling system.* PhD thesis, Mikroelektronik Centret, Tehnical University of Denmark., Lyngby, Denmark, June 2001.

[51] S. D. Senturia. *Microsystem design*. Kluwer Academic Publishers, 2001.

[52] H. J. Ibach. Adsorbate–induced surface stress. *Journal of Vacuum Science and Technology A*, 4:2240–2245, 1994.

[53] J. Fritz, M. K. Baller, H. P. Lang, H. Rothuizen, P. Vettiger, E. Meyer, H.-J. Güntherodt, Ch. Gerber, and J. K. Gimzewski. Translating biomolecular recognition into nanomechanics. *Science*, 288:316–318, 2000.

[54] G. Wu, H. Ji, K. Hansen, T. Thundat, R. Datar, R. Cote, M. F. Hagan, A. K. Chakraborty, and A. Majumdar. Origin of nanomechanical cantilever motion generated from biomolecular interactions. *Proceeding of the National Academy of Sciences of the USA*, 98:1560–1564, 2001.

[55] F. Liu, Y. Zhang, and Z. Ou-Yang. Flexoelectric origin of nanomechanic deflection in dnamicrocantilever system. *Biosensors and Bioelectronics*, 18:655–660, 2003.

[56] A. M. Moulin, S. J. O'Shea, R. A. Badley, P. Doyle, and M. E. Welland. Measuring surface-induced conformational changes in proteins. *Langmuir*, 15:8776–8779, 1999.

[57] A. K. Chakraborty and A. J. Golumbfskie. Polymer adsorption-driven self-assembly of nanostructures. *Annual Review of Physical Chemistry*, 52:537–573, 2001.

[58] S. Tombelli, M. Minunni, and M. Mascini. Analytical applications of aptamers. *Biosensors and Bioelectronics*, 20:2424–2434, 2005.

[59] Institute for Cellular and The University of Texas at Austin Molecular Biology. The ellington lab aptamer database. http://aptamer.icmb.utexas.edu.

[60] M. Liss, B. Petersen, H. Wolf, and E. Prohaska. An apatamer-based quartz crystal protein biosensor. *Analytical Chemistry*, 74:4488–4495, 2002.

[61] M. Lee and D. R. Walt. A fiber optic microarray biosensor using aptamers as receptors. *Analytical Biochemistry*, 282:142–146, 2000.

[62] M. D. Schlensog, T. M. A. Gronewold, M. Tewes, M. Famulok, and E. Quandt. A love-wave biosensor using nucleic acids as ligands. *Sensors and Actuators. B, Chemical*, 101:308–315, 2004.

[63] M. Minunni, S. Tombelli, A. Gullotto, E. Luzi, and M. Mascini. Development of biosensors with aptamers as bio-recognition element: the case of hiv-1 tat protein. *Biosensors and Bioelectronics*, 20:1149–1156, 2004.

[64] T. G. McCauley, N. Hamaguchi, and M. Stanton. Aptamer-based biosensor arrays detection and quantification of biological macromolecules. *Analytical Biohemistry*, 319:244–250, 2003.

[65] Inc. SomaLogic. http://www.somalogic.com/index.html.

[66] J. C. Love, L. A. Estroff, J. K. Kriebel, R. G. Nuzzo, and G. M. Whitesides. Self-assembled monolayers of thiolates on metals as a form of nanotechnology. *Chemical Reviews*, 105(4):1103–1169, 2005.

[67] Analog Devices, Inc. *Interactive Design Tools: Sigma-Delta Analog-to-Digital Converters : Sigma-Delta ADC Tutorial*. http://www.analog.com.

[68] Andrew S. Tanenbaum. *Computer Networks*. Prentice Hall PTR, 4th edition edition, 2002.

[69] *TH72011 433 MHz Transmitter – Datasheet*. http://www.melexis.com.

[70] B. P. Lathi. *Modern Digital and Analog Communication Systems*. Oxford University Press, Inc., 3rd edition edition, 1998.

[71] Theodore R. KuckLick. *The Medical Device R & D Handbook*. CRC Press, 2006.

[72] C. K. O'Sullivan and G. G. Guilbault. Commercial quartz crystal microbalance – theory and applications. *Biosensors and Bioelectronics*, 14:663–670, 1999.

[73] G. Z. Sauerbrey. *Verwendung von schwingquarzen zur wagung dunner schichten und zur mikrowagung.* (The use of quartz crystal oscillators for weighing thin layers and for micro-weighing). *Zeitschrift für Physik*, 155:206–222, 1959.

[74] Stanford Research Systems. QCM100 – quartz crystal microbalance theory and calibration.

[75] A. Mirmoshseni and V. Hassanzadeh. Application of polymer-coated quartz crystal microbalance (qcm) as sensor for btex compounds vapors. *Journal of Applied Polymer Scienc*, 79:1062–1066, 2000.

[76] Y. Fu and Finklea H. O. Quartz crystal microbalance sensor for organic vapor detecion based on molecular imprinted polymers. *Analytical Chemistry*, 75:5387–5393, 2003.

[77] K. H. Karmakar and G. G. Guilbault. A new design and coatings for piezoelectric crystals in measurement of trace amounts of sulfur dioxide. *Analytica Chimica Acta*, 71:419–424, 1974.

[78] Guilbault G. G. and J. H. Luon. Minireview – gas phase biosensors. *Journal of Biotechnology*, 9:1–10, 1988.

[79] G. G. Guilbault, B. Hock, and R. Schmid. Piezoelectric immunosensor for atrazine in drinking water. *Biosensors and Bioelectronics*, 7:411–419, 1992.

[80] M. Plomer, G. G. Guilbault, and B. Hock. Development of a piezoelectric immunosensor for the detection of enterobacteria. *Enzymer Microbial Technology*, 14:230–235, 1992.

[81] B. König and M. Grätzel. Detection of viruses and bacteria with piezoimmunosensors. *Analytical letters*, 26:1567–1575, 1993.

[82] J. S. Boveniser, M. B. Jacobs, G. G. Guilbault, and C.K. O'Sullivan. Detection of pseudomonas aeroginosa using the quartz crystal microbalance. *Analytical Letters*, 31:1287–1295, 1998.

[83] F. Aberl, H. Wolf, C. Kösslinger, S. Drost, P. Woias, and S. Koch. Hiv serology using piezoelectric immunosensors. *Sensors and Actuators B: Chemical*, 18:271–175, 1994.

[84] M. König, B. ad Grätzel. A novel immunosensor for herpes virus. *Analytical Chemistry*, 66:341–344, 1994.

[85] N. C. Fawcett, R. D. Craven, P. Zhang, and J. A. Evans. Quartz crystal microbalance response to solvatedd macromolecules. *Analytical Chemistry*, 70:2876–2880, 1988.

[86] F. Caruso, E. Rodda, D. Furlong, K. Niikura, and Y. Okahata. Quartz crystal microbalance study of dna immobilization and hybridization for nucleic acid sensor development. *Analytical Chemistry*, 69:2043–2049, 1997.

[87] S. Storri, T. Santorini, M. Minunni, and M Mascini. Surface modification for development of piezoimmunosensors. *Biosensors and Bioelectronics*, 13:347–357, 1998.

[88] L. Nie, X. Zhang, and S. Yao. Determination of quinine in some pharmaceutical preparations using a piezoelectric assays. *Journal of Pharmaceutical and Biomedical Analysis*, 10:529–533, 1992.

[89] W. Z. Wei, C. W Hu, W. H. Zhu, and S. Z. Yao. Selective pharmaceutical analysis technique with sensitive piezoelectric quartz sensors. *Analytical Letters*, 26:2371–2383, 1993.

[90] http://www.oligos.com.

[91] http://www.icmfg.com.

[92] Virginia Polytechnic Institute and State University. Alcohol's effects. http://www.alcohol.vt.edu/Students/alcoholEffects/index.htm.

[93] National Highway Traffic Safety Administration. Drugs and human performance face sheets: Cocaine. http://www.nhtsa.dot.gov.

[94] Colin K. Campbell. *Surface Acoustic Wave Devices for Mobile and Wireless Communications*. Academic Press, Boston, MA, 1998.

[95] *CC1020 Low-Power RF Transceiver for Narrowband Systems – Datasheet*.

[96] GE Healthcare Life Sciences. Disposable pd-10 desalting columns. http://www6.gelifesciences.com/.

Appendix

Appendix A: Base Station

The base station of the sensor performs the following tasks:

1. Detect and receive RF signal at the specified frequencies,
2. Demodulate the baseband signal,
3. Convert signal into a digital serial bit stream,
4. Capture and hold the digital package,
5. Perform decoding and format the data for transfer to host,
6. Hold packet in small FIFO to handle interrupt latency of host,
7. Interrupt host to inform of packet available, and
8. Transfer packet on host command.

The base station consists of an external antenna, a 50 Ω RD input interface, a filter, an RF receiver, a controller, and a serial interface for connection to a PC as user interface as illustrated in Fig. 1.

Filter

Signal filtering is performed using Surface Acoustive Wave (SAW)-based filter, B3550, manufactured by Epcos, Inc.. The component is chosen as the filter for the base station due to its selectivity (good ultimate rejection), low loss characteristic with high quality factor

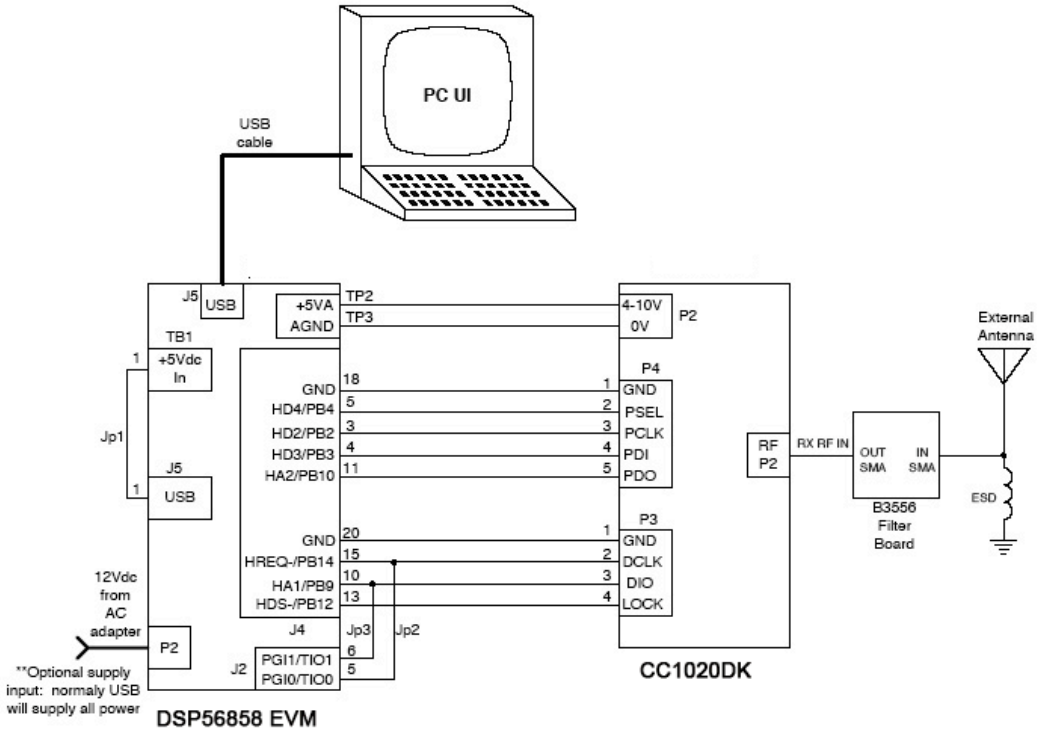

Figure 1: Base station block diagram.

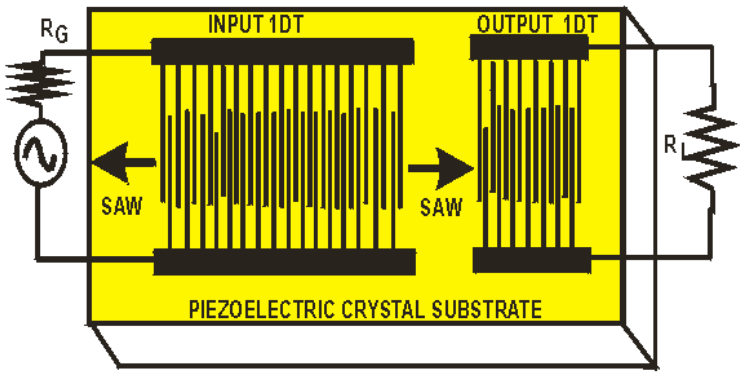

Figure 2: Basic SAW interdigital transducer structure on piezoelectric substrate.

"Q", and low coefficient of thermal expansion that provides stable frequencies over a wide temperature range. The filter center of frequency is 403.55 MHz between 3dB points. In general, a SAW filter consists of one input and on output interdigital transducers (IDTs). An interdigital transducer is a comb-shaped evaporations of metal on a piezoelectric substrate as illustrated in Fig. 2 [94]. The SAW filter converts an electrical signal at the input IDT into a mechanical surface wave. The mechanical surface wave then propagates on the substrate surface to the output IDT to be converted back to the electrical signal.

Receiver

CC1020 transceiver chip from Texas Instruments is used as the RF receiver. This component is decided due to its low power, low voltage wireless RF transceiver, short range device frequency bands, suited for narrowband systems, and mainly intended for industrial, scientific, and medical purposes. In addition, the CC1020 also performs FSK modulation and demodulation, Manchester encoding and decoding, and data synchronization. Currently, a unidirectional communication from sensors to the base station instead two-way communication is used to maximize the battery life and minimize the complexity of the system. The CC1020 is programmed as a receiver mode by a microcontroller that is connected to it. Fig. 3 [95] shows the block diagram of the receiver (highlighted part). RF input signal is first amplified by the low noise amplifier and then down-coverted in quadrature to the

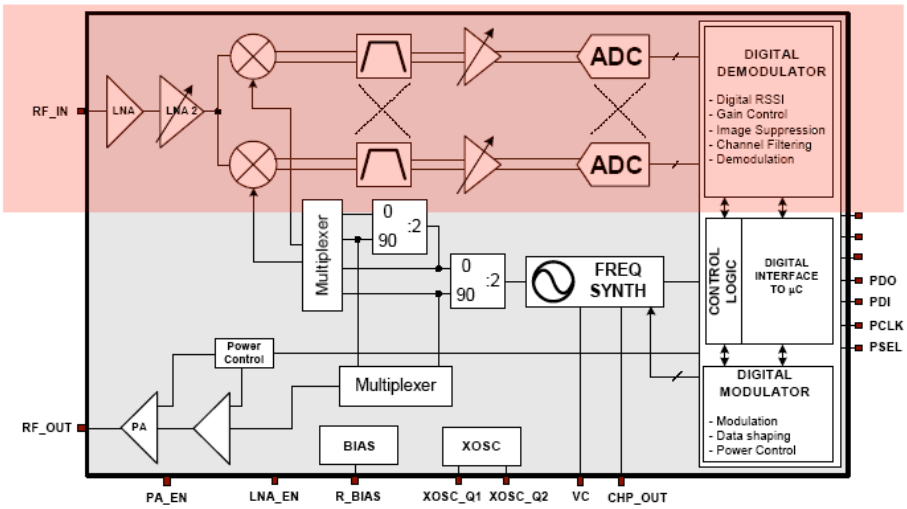

Figure 3: CC1020 transceiver block diagram. The highlighted part is the receiver diagram [95].

intermediate frequency. After being filtered and amplified, the IF signal is then digitized by the ADCs and passed to the digital demodulator. The demodulator block diagram is described in Fig. 4 [95]. It has a built-in bit synchronizer which synchronizes the internal clock and the incoming data, and performs data decoding. Outputs of the digital demodulated data is sent out on the DIO pin while the synchronized data clock is available at the DCLK pin.

The transceiver chip also provides a built-in Received Signal Strength Indicator (RSSI) and allows connection to a microcontroller. In our sensor application, RSSI is used to inform when to begin decoding the received RF signal from the sensor.

Controller

The component selected as the microcontroller is DSP56858 from Motorola, Inc. The controller is a combines of digital signal processor and microcontroller in a single chip to reduce cost. However, for the sensor project only the microcontroller function is applied to

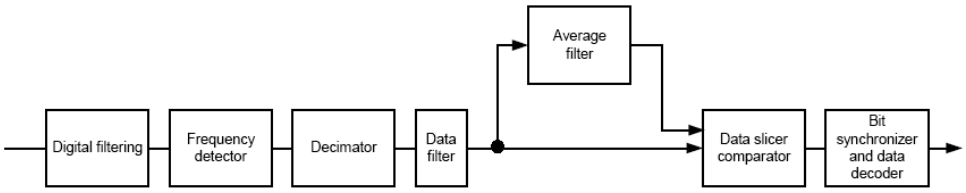

Figure 4: CC1020 demodulator block diagram [95].

handle RS232 communication, read the decoded packets from the receiver, and then send them to the PC.

RF Link Protocol

The communication between the transmitter/sensor and the receiver/base station is done unidirectional to maximize battery life and reduce system complexity. Although in the future both direction of communication between the sensor and the base station can be implemented. The sensor only transmits its packet data during its designated time slots, which is pseudo-randomized to reduce the incidence of collisions among co-located sensors. The initial time synchronization of sensor and base station, called the **Marriage** process, consists of the following:

1. Base station is placed in a Marriage mode, in which the receiver is set on continuously and the base station monitors the contents of the register signal strength indicator (RSSI) of the sensor to be married,

2. The sensor is activated and placed in proximity to the base station,

3. When base station detects increase in the RSSI level, which is computed from the RSSI register in the sensor data packet, it shall begin decoding the received RF signal,

4. If the decoded packet is invalid, that is the decoded bit errors is greater than 0, the base station remains in continuous listen model until packet is error free,

5. If the decoded packet is valid, the base station extract sensor ID and the sensor pseudo-random time slow or window sequence, and introduce the sensor to the network,

6. The base station continues to monitor the married sensor along with other married sensor once the Marriage process is successful.

If there is loss in communication between the sensor and the base station, resynchronization is not required. The base station continues to listen for sensor packet at the computed time slots until commanded to drop the sensor from the network.

Appendix C: Flow channel fabrication

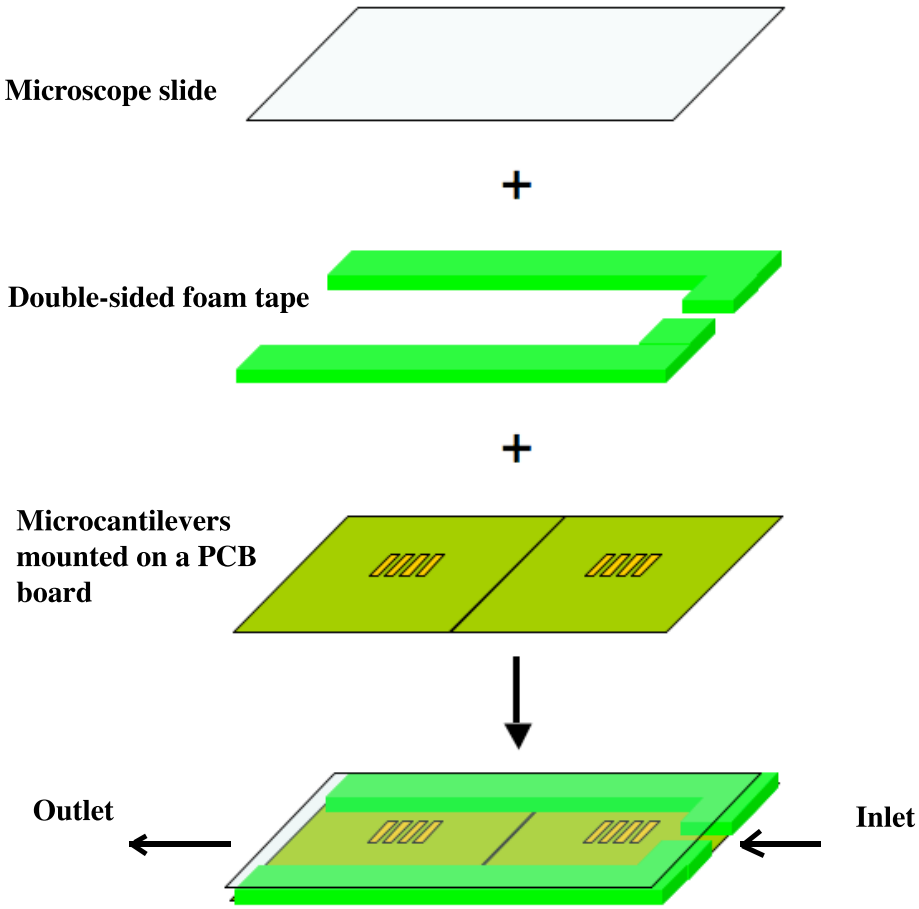

Figure 5: Fabrication procedure of the flow channel used by the sensors in the flow controlled system

Appendix D

Deprotecting procedure of thiolated oligonucleotide-based aptamer

The procedure is based on the the Oligos, Inc. website [90] that has been customized to the amount of aptamer that we received from the company. We received two vials.

Quantity of each vial:

(a) μg/vial = 7807.1

(b) nmole/vial = 636.0

(c) A260/vial = 286.0

The following procedure is performed only to one vial.

1. Add 2.86 ml of 0.1 M triethylammonium acetate (TEAA) buffer, pH 6.5, to resuspend the lyophilized oligonucleotide in at a concentration of approximately 100 A260 units/milliliter.

2. Add 429 μl of 1M aqueous silver nitrate solution ($AgNO_3$) to the solution **1**, mix thoroughly, and leave to react at room temperature for 30 minutes.

3. Add 572 μl of 1M aqueous DTT (dithiothreitol) solution to the solution **2**, mix thoroughly, and leave at room temperature for 5 minutes.

4. Centrifuge the suspension in **3** at 4K rpm for 10 minutes to remove the silver-DTT complex.

5. Remove and keep the supernatant (the top layer in the vial) using a pipette.

6. Wash the precipitate in **5** with 2.86 ml of 0.1 M TEAA.

7. Centrifuge **6** also at 4K rpm for 10 minutes.

8. Combine the supernatant in **7** with that in **5**.

9. Centrifuge the total supernatant again at 4K rpm for 3 minutes to ensure no precipitation in the solution. If there is precipitation, carefully separate the supernatant and place it in a new vial.

10. Perform gel filtration to the supernant using PD-10 column [96].

Note: If this free thiol oligonucleotide is not to be used immediately, it should be stored under an inert atmosphere to avoid oxidative dimerization to the disulfide.

Vita

Bernadeta Srijanto was born in Kuala Lumpur, Malaysia, on December 27, 1973, and moved to Salatiga, Indonesia in 1979. After graduated from SMA Negeri 1 Salatiga, she studied at Gadjah Mada University in Yogyakarta. In August 1993, she was transferred to the University of Tennessee at Knoxville, where she received her Bachelor of Science degree in Electrical and Computer Engineering in May 1998. During her undergraduate studies she worked for Philips Consumer Electronics as a student intern and for the Office of Information Technology at the University of Tennessee, Knoxville, as a student assistant. She then continued her master degree in Electrical Engineering which she completed in May 2002. While pursuing her master degree, she was a graduate teaching assistant for the Electrical and Computer Engineering Department and a research assistant for the Microelectronic Systems Research Laboratory. Later, Bernadeta began working toward her Doctor of Philosophy degree started in August 2003. She worked as a research assistant at the Molecular Bioscience and Biotechnology Group in Oak Ridge National Laboratory for two years. In 2005 she joined the Applied Physics Laboratoy group at the Physics Deparment. She was also a graduate teaching assistant for the Electrical Engineering and Computer Science Department. She received her Doctor of Philosophy degree in Electrical Engineering in May 2008.